Isomorphs and pseudoisomorphs

A PhD Thesis

BY

Andeas Elmerdahl Olsen
Supervisor: Thomas Schrøder

August 12, 2016

Danish National Research Foundation Centre *Glass and Time*,
IMFUFA, Department of Science and Environment,
Roskilde University, Denmark

Abstract

The present thesis deals with the scientific field of glass and viscous liquids, and in particular the isomorphs theory, through the application of computer simulations. The thesis is divided into two main contributions.

In the first part, the isomorph theory is applied to classical crystalline systems, in particular the single component Lennard-Jones fcc crystal, showing that even though the theory was developed for liquid systems, it works even better for crystalline systems. This is further confirmed by the investigation of six other model systems, two of which do not have isomorphs in the liquid phase; it is shown that systems without isomorphs in the liquid phase do not have isomorphs in the crystal phase either.

The second part of the thesis introduces the notion of pseudoisomorphs, characterizing systems without isomorphs but with isomorph-like behavior. These have been found in model systems with bonded interacts modeled as harmonic springs. Two methods for identifying pseudoisomorphic state points are developed and presented. The first relies on the fact that for the models used in this thesis, the eigenvalues of the potential energy Hessian fall into two distinct parts, one that corresponds to the harmonic bonds and one that corresponds the remaining degrees of freedom. It is shown that the latter of these scale in accordance with the isomorph theory. The second method is of a more general nature, equating the reduced free energy of a system at different state points. Both methods leads to a number of implementations for identifying pseudoisomorphs. The methods are applied to two specific model systems, a simple asymmetric dumbbell model and a 10-bead Lennard-Jones chain model. Pseudoisomorphs are successfully found for both models.

Resume

Denne afhandling omhandler glasser of viskøse væskers, og i særdeleshed isomorfteorien, gennem anvendelse af computersimuleringer. Afhandlingen falder i to hoved bidrag. I den første del anvendes isomorfteorien på klassiske krystallinske systemer, i særdeleshed en-type Lennard-Jones fcc krystallen, og det vises, at selv om teorien blev udviklet til væskesystemer virker den endnu bedre for krystallinske systemer. Dette underbygges yderligere af en undersøgelse af yderligere seks krystallinske modelsystemer, af hvilke to ikke har isomorfer i væskefasen. Det bliver vist, at systemer derikke har isomorfer i væskefasen heller ikke har det i den krystallinske fase.

Den anden del af afhandlingen introducerer ideen om pseudoisomorfer, systemer uden isomorfer men med isomorf-lignende opførsel. Disse er blevet fundet for modelsystemer med interaktioner modeleret som harmoniske fjedre. To metoder udvikles til at identificere pseudoisomorfe tilstandspunkter. Den første anvender det faktum, at for modellerne anvendt i denne afhandling vil egenværdierne af en potentielenergi Hessian dele sig i to grupper, en der knytter sig til de harmoniske bånd i modellen og en der knytter sig til de resterende frihedsgrader. Det vises, at den anden af disse grupper skalerer i overensstemmelse med isomorfteorien. Den anden metode er af en mere generel natur. Den finder tilstandspunkter med den samme reducerede fri energi. Begge metoder anvendes på to specifikke modelsystemer, en simpel asymmetrisk to-partikel model og en 10-partikel Lennard-Jones kæde. Der findes pseudoisomorfer for begge modeller.

Acknowledgements

First I would like to thank my superviser Thomas for his great guidance and involvement. Secondly I would like to thank inparticular Jeppe but also the rest of the Glass and Time group for their help and inputs. A special thanks to Lorenzo who have been with me on this journey, through the last three years.

I would never have been able to do this with out the support of my girlfriend Tine who, in particular near the end, have been a pillar of calm and sanity in my world. Thank you.

Finally a thank you to IMFUFA in general. An institution that has been the basis for my everyday life for nearly a decade.

The image on the front page is of "Sneglen" ("The Snail"), an outdoor swimming facility not far from where I live. Thank you Per.

Contents

1 Glass and viscous liquids

This chapter gives a very brief introduction to the research of the glass transition and viscous liquids, since these are the main focus of the "Glass and Time"-group at Roskilde University and has played an important role in leading to the results in this thesis. Many excellent overviews of this have been made trough the time, see for instance [14, 15, 20, 46], so this chapter will aim to introduce the different concepts of the subjects.

1.1 Glass and the glass transition

Though glass is a common everyday object, it is almost solely associated with the transparent, solid material used in windows and containers. While this is indeed a glass it is far from the only one.

In a scientific sense being a glass is a state of matter much like being a liquid or a gas, but with some striking differences. A glass is defined as an amorphous solid system meaning that the atoms or molecules of the system are disordered, like in a liquid, but does not flow on any measurable time scale. A glass can be formed from many different types of substances, from organic molecules to metallic alloys and though methods for production of glass dates back at thousands of years, the glass state and in particular the glass transition are relatively new fields of science, and it is still with out an explanation.

In general a glass is formed by cooling a liquid with a high cooling rate, where "high cooling rate" depends on the liquid. Other methods exists for forming glasses, but this is the most common. When a liquid is cooled it will solidify usually by forming a crystal at a specific temperature T_m where the particles of the liquid forms a lattice structure of some kind. This is a result of the crystal structure being thermodynamically more stable at temperatures below T_m. If a liquid is cooled too fast, this crystallization can be avoided and the liquid can be brought to temperatures below T_m, at which point the liquid is said to be super cooled. The cooling rates needed for this can for some liquids be so high that they cannot yet be reached, where for other liquids it is so low, that obtaining crystallization can be problematic.

If the liquids is further cooled at this high cooling rate, the dynamics of the liquid will start to slow down, due to the lack of kinetic energy. Eventually, the dynamics will be so slow, that the system is no longer able to equilibrate even partially. After

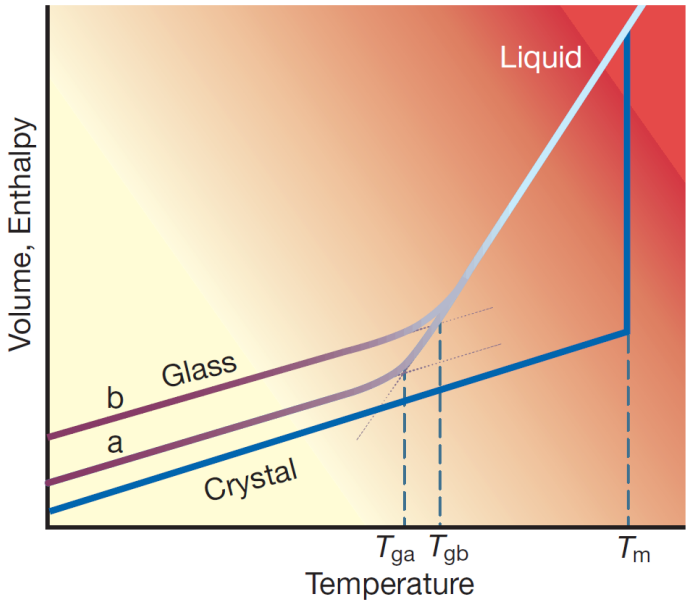

Figure 1.1: Illustration of the liquid to crystal and liquid to glass transition shown as enthalpy or volume as a function of temperature. The system starts as liquid in the top right corner of the figure. At low cooling rate the system will begin to crystallize once it reaches the temperature T_m, characterized by a isothermal change in enthalpy or volume. Bringing the temperature of the system further down will only result in a "deeper" crystal phase. If the liquid is cooled too fast it will not crystallize but instead continue on the liquid state curve until it reaches a temperature T_g where it can no longer reach equilibrium and becomes a glass. This glass transition temperature depends not only on the liquid but also on the cooling rate. The figure is taken from [14].

this the system is considered a glass and the temperature at which this occurs is called the glass transition temperature T_g. The figure 1.1 illustrates this process. A liquid is cooled and as it reached the melting temperature T_m it either starts crystallizing, resulting in a isothermal change in volume or enthalpy, or it continues on the liquid curve if the cooling rate is high enough. Once it falls out of equilibrium there is a change in the enthalpy or volume slope, signifying the glass transition temperature T_g. Contrary to for instance the melting temperature T_m which for a given liquid is function only of pressure or density, the glass transition temperature is also a function of the cooling rate, with higher cooling rate giving higher values of T_g.

1.2 Viscous liquids

In order to understand the glass state and transition, a lot of research have been done on the super cooled liquids, often referred to as viscous liquids, due to their very slow

dynamics or high viscosity. Contrary to the glasses themselves, the viscous liquids are in equilibrium meaning that ordinary thermodynamics can be used in dealing with these. Further more, the glass transition temperature is not uniquely defined, a problem that is avoided by working with the viscous liquid.

One of the main focuses of this research has been to understand the large increase in viscosity or slow down of dynamics that happens even for small changes in temperature as the liquid approaches the glass transition where "Small changes in thermodynamic conditions can alter the time scale for molecular motions from nanoseconds to a duration exceeding the human lifespan" [46]. Such a slow down is often described with a relaxation time τ, a measure of how long it takes the system to equilibrate. One can imagine perturbing a system somehow, and then measure the time it takes the system to re-equilibrate. This would give a measure of the relaxation time.

The problem of understanding the change in relaxation time for viscous liquids near the glass transition is further complicated by the observation that τ also increases drastically if the system is compressed under constant temperature, instead of cooled under constant pressure p or density ρ making the problem two dimensional, $\tau = \tau(\rho, T)$ and that these changes are system dependent.

2 Simulation methods

This chapter is meant to give an introduction to computer simulations of atomistic and molecular model systems. Several good books have been written to cover this in great detail, see for instance [2, 22, 42], so this will be a very short introduction focusing on the aspects and methods used in this thesis.

2.1 Molecular dynamics

Far most of the results presented in this thesis where made using molecular dynamics simulations where Newton's equations of motion are solved numerically.

We imagine a set of N particles represented by their position $\mathbf{R}(t) = (\mathbf{r}_1(t), \mathbf{r}_2(t), \ldots, \mathbf{r}_N(t))$ and their velocities $\mathbf{V}(t) = (\mathbf{v}_1(t), \mathbf{v}_2(t), \ldots, \mathbf{v}_N(t))$.

In order to have any interaction between particle, we define a potential energy $U(\mathbf{R})$. Such an energy can be expressed in many different ways, but commonly and in this thesis the potential energy is taken as a sum over pair interactions

$$U(\mathbf{R}) \equiv \sum_{i=1}^{N} \sum_{j>i}^{N} u(r_{ij}) \tag{2.1}$$

where r_{ij} is the distance between particle i and j.

A classic example of such a pair potential is the Lennard-Jones potential [34]

$$u_{ij}(r_{ij}) = 4\epsilon_{ij} \left[\left(\frac{\sigma_{ij}}{r_{ij}} \right)^{12} - \left(\frac{\sigma_{ij}}{r_{ij}} \right)^{6} \right] \tag{2.2}$$

where ϵ_{ij} is a characteristic energy that gives the relative strength of the interaction between particles of type i and j and σ_{ij} is a characteristic length of this interaction. Specifically the minimum energy of this potential is $-\epsilon$ and the energy is zero at $r = \sigma$. The figure 2.1 shows the potential energy of the Lennard-Jones potential as a function of pair distance r. The potential is characterized by a short range repulsion from the r^{-12}-term (Pauli exclusion) and an attraction at longer ranges from the $-r^{-6}$-term (van der Waals attraction). These are separated by the energy minimum, giving the optimal pair distance for a pair of particles in isolation. At very long distances the potential energy and the force both goes to zero. This potential is used extensively in this thesis.

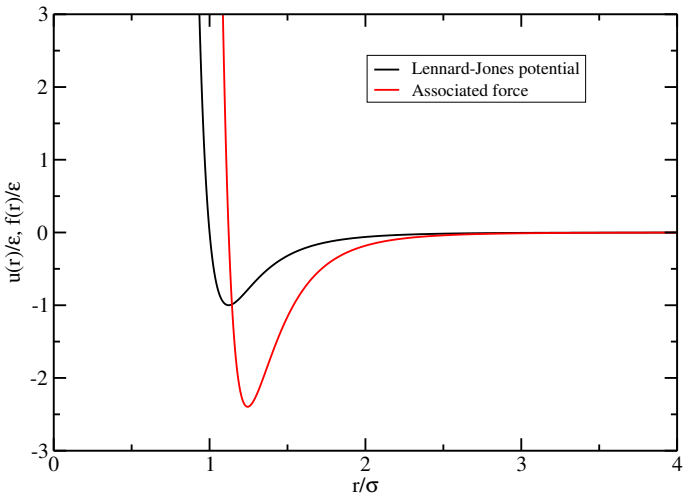

Figure 2.1: The Lennard-Jones potential and the size of the associated force as a function of the pair distance r. This potential is a classic example of a pair potential used in molecular dynamics simulations.

From the potential it is possible to extract an associated force as the gradient of the potential energy

$$\mathbf{F} \equiv -\nabla U(\mathbf{R}) \tag{2.3}$$

where the potential energy U is defined as above. This implies that the force is given by a set of pair forces, e.g. $\mathbf{f}_{ij}$, the force on particle i from particle j.

For the Lennard-Jones potential this is

$$\mathbf{f}_{ij}^{\mathrm{LJ}}(\mathbf{r}_{ij}) = -24\epsilon_{ij}\left[2\frac{\sigma^{12}}{r_{ij}^{13}} - \frac{\sigma^{6}}{r_{ij}^{7}}\right]\hat{\mathbf{r}}_{ij} \tag{2.4}$$

where $\hat{\mathbf{r}}_{ij}$ is the unit vector pointing from particle i to particle j. The size of the force associated to the Lennard-Jones potential is also included in figure 2.1, with repulsive forces corresponding to positive values on the y-axis.

The total force on a particle is obviously the sum of these

$$\mathbf{f}_i = \sum_{j \neq i} \mathbf{f}_{ij}(\mathbf{r}_{ij}) \tag{2.5}$$

From Newton's equation of motion we have

$$\frac{d\,\mathbf{r}_i}{d\,t} = \mathbf{v}_i(t) \tag{2.6}$$

and

$$\frac{d\,\mathbf{v}_i}{d\,t} = \frac{\mathbf{f}_i(t)}{m_i} \tag{2.7}$$

To use this in molecular dynamics simulations, we need to discretize the time which can be done in a number of ways. Here we do it with the leap-frog algorithm based on the very common Verlet algorithm [68]. If we imagine that time is discretized around a specific time t with time steps Δt, e.g. $\ldots, t-2\Delta t, t-\Delta t, t, t+\Delta t, t+2\Delta t, \ldots$, we calculate the position and force at these time steps, $\ldots, \mathbf{R}(t-\Delta t), \mathbf{R}(t), \mathbf{R}(t+\Delta t), \ldots$. The velocities are not calculated at the time steps but rather at the intermediate half-step $\ldots, \mathbf{V}(t-\Delta t/2), \mathbf{V}(t+\Delta t/2), \ldots$. This introduction of intermediate half-steps is what prompted the name "leap-frog" and is where the algorithm deviates from the original Verlet algorithm. The leap-frog algorithm is mathematically equivalent to the original Verlet algorithm but is generally more stable in computer simulations.

The time evolution of a particle in the system is as follows,

$$\mathbf{v}_i(t+\Delta t/2) = \mathbf{v}_i(t-\Delta t/2) + \Delta t \frac{\mathbf{f}_i(t)}{m_i} \tag{2.8}$$

$$\mathbf{r}_i(t+\Delta t) = \mathbf{r}_i(t) + \Delta t \mathbf{v}_i(t+\Delta t/2) \tag{2.9}$$

after which the new forces $\mathbf{F}(t+\Delta t)$ can be evaluated from the updated position.

Since velocity and position are not know at exactly the same time, the total energy of the system is not know. In order to resolve this one takes as the velocity $\mathbf{v}(t)$ the mean of the velocities immediately before and after

$$\mathbf{v}_(t) = \frac{\mathbf{v}(t-\Delta t) + \mathbf{v}(t+\Delta t)}{2} \tag{2.10}$$

2.2 Monte Carlo simulations and Metropolis algorithm

An alternative to molecular dynamics simulations is to use Monte Carlo methods, that relies on repeated random sampling. The name, Monte Carlo, is a reference to this randomness. In the context of computer simulations of classical mechanical systems, this is often done with the Metropolis algorithm [37]. The basic algorithm is as follows:

Start with a set of particle positions $\mathbf{R}(t)$ (for the sake of this thesis, the velocities are not used in the Monte Carlo simulations) from which we evaluate a potential energy $U(t)$. Perform a trial move by displacing the system $\mathbf{R}^* = \mathbf{R}(t) + \delta\mathbf{R}$ and evaluate a trial potential energy $U^* = U(\mathbf{R}^*)$. Most often $\delta\mathbf{R}$ will be a displacement of one or all of the particles. The system will change into this trial state with the probability

$$P(\mathbf{R} \to \mathbf{R}^*) = \begin{cases} \exp\left[-(U^* - U(t))/k_B T\right] & \text{if} \quad U(t) < U^* \\ 1 & \text{else} \end{cases} \tag{2.11}$$

meaning that a system always goes to a state with lower energy if possible and will perform a move to a higher energy state with a probability given by the relative Boltzmann probabilities of the two states. The advantage of this way of sampling the configurational space is, that the micro configuration visited are visited a number of times proportional to their actual probability meaning that one does not have to calculate the Boltzmann probability of every micro configuration in order to find the more probable ones.

Unlike the molecular dynamics simulations, this method does not access the instantaneous dynamics of the system. The "time" t is not a time as such, since the configuration at time $t + \Delta t$ is not uniquely given from the configuration at time

t. There are however no problem in using this method to estimate different average thermodynamic quantities like $\langle U \rangle$ and long time dynamical behaviour like the diffusion constant.

The advantage of this method and the reason it is used here is that it allows for a very easy control over which micro configurations to visit and in turn to calculate an average over. If for instance one wants to keep a set of particles fixed at their current location one can simply configure the program to sample only those micro configurations and be certain that the averages calculated will be an approximation to the correct averages in that particular subspace of the configurational space. This will be done in section 7.4 where a molecular systems is investigated and an average is calculated over micro configurations with a specific orientation and center-of-mass position of each molecule. Conversely, formulating a self consistent, time reversible molecular dynamics algorithm for doing this is quite difficult.

2.3 Practical considerations

One clear disadvantage of computer simulations over experiments is the ratio between real and simulated time. There are different ways to address this problem.

Defined as above, the forces or energies have to be calculated at each time step as a sum over all particle pairs, meaning N^2 calculation per time step. This can be reduced greatly by making a cut-off in the pair potentials and forces. The Lennard-Jones potential goes to zero at large pair distances, and the dynamics are largely dominated by short range interactions. By truncating the energy or force at a specific distance one still get the same dynamics without a large part of the N^2 calculations. The classic procedure is to truncate and shift the pair potential at a cut-off distance r_C

$$u_{\mathrm{SP}}(r) = \begin{cases} u(r) + u(r_C) & \text{if } r < r_C \\ 0 & \text{else} \end{cases} \tag{2.12}$$

where r_C depends on the specific potential. As an alternative to this one can truncate and shift the pair force in a similar manner, which have been shown to allow for shorter cut-off distances [58]. This allows for calculating the interactions only for particles that are within the cut-off. To gain anything from this one of cause needs to keep check on which particles are within the cut-off, something that are taken care of by the use of neighbour lists.

Since the system size in computer simulations are very small compared to experimental system one need to be careful in order to obtain bulk behaviour, if that is in fact the aim of the simulation. In order to do this one can use periodic boundaries, where the system is replicated in each direction. The particles are allowed to interact with particles in these replicas through the pair potentials and if a particle leaves the simulation box it is automatically replaced by another particle entering from one of the replicas. To avoid particles interacting with themselves or with a particle and a replicate of the same particle, periodic boundaries can be used together with a cut-off in potential or force that is less than half the minimal length of the simulation box. This criteria is also referred to as the minimal image convention, meaning that particle i interact with another particle j with a distance r_{ij} given by the minimal distance between particle i and all copies of particle j.

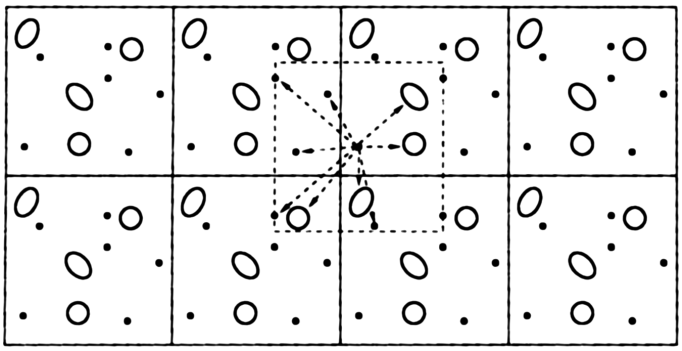

Figure 2.2: Illustration of the periodic boundary conditions used in many simulations to get bulk behaviour from "small" systems. The simulation box is replicated in each direction and the particles can feel these replicas and is allowed to exit the simulation box, since a particle that moves out of the simulation box is replaced by one entering from another replica. Taken from [22].

2.4 GPU computing and RUMD

One huge leap in the efficiency of computer simulations like those described here came with the introduction of NVIDIA's CUDA programming environment. This was created to allow people to write programs that utilized the calculation capabilities of the graphics cards, the GPUs – Graphics Processing Units. An ordinary computer program runs on the CPU, Central Processing Unit, which is capable of efficiently handling a number of difficult calculations requiring large amount of memory. The GPU, on the other hand, has a huge number of cores, each capable of handling a single calculation, given that it is not too memory consuming, e.g. what to display in a single pixel on the screen. This makes it ideal for calculating for instance the distance between two particles and thus the force between them since this is a very simple calculation, and one that needs to be done many times per time step during a computer simulation.

This have been used in the Roskilde University Molecular Dynamics program RUMD [7]. It is an open source molecular dynamics program, that has been optimized for long simulations of smaller systems. This is seen of figure 2.3, where the number of time steps performed per second is shown as a function of system size. The figure compares the RUMD simulation program to the well know computer simulation program LAMMPS and it is clear that RUMD is better at small system sizes and that the two programs are comparable at larger sizes. By using smaller system sizes one can get a higher simulated time to real time ratio, making it possible to better probe the long time dynamics of viscous liquids. Further more, RUMD allows for relatively simple manipulation of most parts of the simulation procedures, something that was used in the work presented in chapter 7.

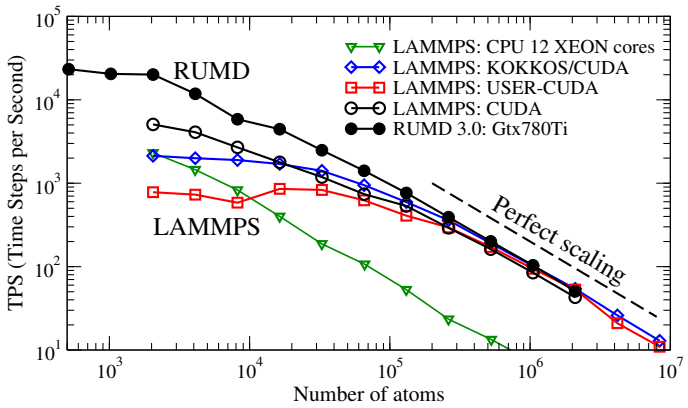

Figure 2.3: The number of time steps performed per second for the RUMD simulation program, compared to one of the well known simulation programs, LAMMPS, as a function of system size. RUMD greatly out perform LAMMPS at small systems sizes, and they are comparable at larger sizes. The figure is taken from [7].

Part I

Roskilde systems and isomorphs

3 Roskilde systems

This chapter introduces the notion of a Roskilde simple system and the isomorph theory. The offset is empirical density scaling, where the isomorph theory is introduced as an explanation for this. Since the conception of the isomorph theory in [23] the theory have been tested extensively. For a review of the applications and implications of the theory we refer to the feature article [17]. The theory have also been reformulated [52]. It is this reformulation that is the basis of the presentation here.

3.1 Empirical power law density scaling

Though there are still no full explanation for the strong state point dependence of the dynamics of viscous liquids, for a class of systems, the problem has been made simpler. It was found experimentally by Tölle *et al.* [56, 57] that for ortho-terphenyl, the dynamics is not a function of density and temperature independently but rather a specific combination of the two, $\tau = \tau(h(\rho)/T)$ with $h(\rho) = \rho^4$. This effectively reduces the two dimensional (ρ, T)-phase space to a one dimensional one, meaning that the relaxation calculated at different points in the (ρ, T)-phase space can be collapsed onto a single curve when plotted as a function of $h(\rho)/T$. The result signifies a certain simplicity of the system and it turns out, that this simplicity is present in a wide variety of systems when $h(\rho)$ is taken as a power law function with a system dependent scaling exponent γ [46].

The property of empirical density scaling is now widely used in a large class of different types of systems, such as small molecular glass formers, polymers, ionic liquids as well as liquid crystals, see for instance [12, 36, 45].

3.2 Strongly correlating liquids and isomorphs

The isomorph theory is a theory that explains the scaling behaviour for a large class of systems by comparing the energy landscape of given system at different state points.

The theory originated in 2008 [5,39], where it was shown that some systems have a high correlation between fluctuations in potential energy U and the configurational part of the pressure, the virial W, defined from $pV = nk_BT + W$, and microscopically

related to the potential energy as, see for instance [26],

$$W(\mathbf{R}) = -\frac{1}{3}\mathbf{R}\cdot\nabla U(\mathbf{R}) \tag{3.1}$$

The correlation was calculated from a standard Pearson correlation

$$R \equiv \frac{\langle \Delta U \Delta W\rangle}{\sqrt{\langle(\Delta U)^2\rangle\langle(\Delta W)^2\rangle}} \tag{3.2}$$

and the discovery led to the definition of strongly correlating liquids, defined as those liquids with a correlation above the somewhat arbitrary threshold $R > 0.9$ [5].

Further investigation of the strongly correlating liquids have resulted in the discovery, that these systems have curves in part of their (ρ, T)-phase space, along which, the dynamics and structure are invariant when measured in macroscopically reduced units [6, 23, 50, 51], meaning that the quantities are reduced by the macroscopic variables density, temperature and mass. We denote these with a tilde. Taking as examples length r, the potential energy U, time t and the diffusion constant D, we have the reduced quantities

$$\tilde{r} = r\rho^{1/3}, \quad \tilde{U} = \frac{U}{k_B T}, \quad \tilde{t} = t\rho^{1/3}\sqrt{\frac{k_B T}{m}}, \quad \tilde{D} = D\rho^{1/3}\sqrt{\frac{m}{k_B T}} \tag{3.3}$$

These lines of invariant structure and dynamics where called isomorphs and systems with such lines are referred to as Roskilde-simple systems or simply Roskilde systems. The theory have been tested for a large class of system including simple atomic systems with quite a broad array of interactions and in both liquid and solid states [1, 16, 23, 27, 67], some small stiff molecules [23, 28] as well as a flexible Lennard-Jones chain [65]. Further more the theory have been tested experimentally with success for van der Wall liquids [24, 44, 71].

3.3 Isomorph theory

There are two equivalent ways of defining isomorphs and they both deal with reduced micro configurations.

We denote a micro configuration by $\mathbf{R}$ meaning the coordinates of all particles $\mathbf{R} = (\mathbf{r}_1, \mathbf{r}_2, \ldots, \mathbf{r}_N)$. A reduced micro configuration $\tilde{\mathbf{R}}$ is the micro configuration scaled to unit density $\tilde{\mathbf{R}} = \rho^{1/3}\mathbf{R}$ to make it a dimensionless quantity.

Included here for completeness follows the two definitions following the derivations of the paper by Schrøder and Dyre (2014) [52].

In deriving the following relations it is important to note, that the isomorph theory is an approximate theory. This means that we do not expect it to hold perfectly, but rather to a good approximation.

Further more, when discussing specific micro configurations $\mathbf{R}$ it is understood, that only the physically relevant ones are considered. For instance there is no claims on the behaviour of the micro configurations with all particles located in a small subvolume of the total system volume, and so forth.

Scaling of energy surfaces

The first way of defining isomorphs are through the direct comparison of the potential energy surface at two different state points.

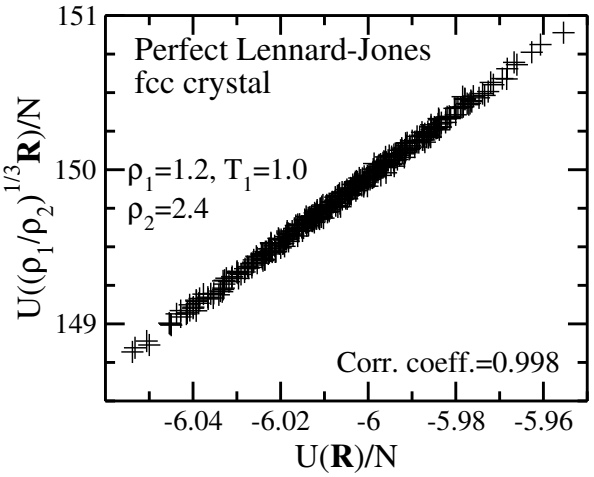

Figure 3.1: The potential energy of a perfect crystalline system with particles interacting via a Lennard-Jones potential. The x-axis is the potential energy of each micro configuration at $(\rho_1, T_1) = (1.2, 1.0)$. Each micro configuration have been scaled to a different density, $rho_2 = 2.4$ and the potential energy calculated for the scaled micro configurations. These are given as the y-axis. The high collapse shows that the energies at the two densities are related in some way. Reproduced from [1].

Two state points, (ρ_1, T_1) and (ρ_2, T_2) are isomorphic if there to a good approximation exists a mapping between the potential-energy surfaces at ρ_1 to that at ρ_2,

$$U(\mathbf{R}_2) \cong f_1(\rho_2, U(\mathbf{R}_1)) \tag{3.4}$$

where $\mathbf{R}_1$ and $\mathbf{R}_2$ have the same reduced coordinates, i.e. $\rho_1^{1/3}\mathbf{R}_1 = \rho^{1/3}\mathbf{R}_2 = \tilde{\mathbf{R}}$ [52]. An example of this is shown on figure 3.1, where the energies $U(\mathbf{R}_2)$ and $U(\mathbf{R}_1)$ are plotted against each other for a perfect Lennard-Jones crystal. This system will be investigated in detail in chapter 4.

From this we can derive a number of invariant quantities for state points that are isomorphic.

By tailor expansion of equation (3.4) to first order in $U(\mathbf{R}_1)$, we get

$$U(\mathbf{R}_2) \cong U(\mathbf{R}_1)\left(\frac{\partial f_1(\rho_2, U(\mathbf{R}_1))}{\partial U(\mathbf{R}_1)}\right)_{\rho_1,\rho_2} + g_1(\rho_2) \tag{3.5}$$

which shows that for small density changes the energy landscape changes by a linear, affine transformation.

In the original formulation of the isomorph theory [23], this first order approximation was taken to be the exact formulation of the scaling between state points, though at that point it was not thought of as a first order expansion. From figure 3.1 it also seems that the potential energies are in fact linearly dependent. Further simulation have however shown that this is not the case [52]. Because of this, a lot of the isomorphic invariances that have been derived, are derived from the first order

expansion. In particular if we choose the temperature T_2 so it is related to T_1 by

$$T_2 = h_1(\rho_2)T_1 \tag{3.6}$$

where

$$h_1(\rho) \equiv \left(\frac{\partial f_1(\rho_2, U(\mathbf{R}_1))}{\partial U(\mathbf{R}_1)} \right)_{\rho_1,\rho_2} \tag{3.7}$$

we get from equation (3.5)

$$U(\mathbf{R}_2) \cong \frac{T_2}{T_1} U(\mathbf{R}_1) + g_1(\rho_2) \tag{3.8}$$

which in turn implies the original isomorph relation presented in [23], comparing the Boltzmann factors of micro configurations with the same reduced coordinates. There two state points (ρ_1, T_1) and (ρ_2, T_2) are isomorphic if, whenever two micro configurations $\mathbf{R}_1$ and $\mathbf{R}_2$ at those state points has the same reduced coordinates they also have proportional Boltzmann factors to a good approximation

$$\exp[-U(\mathbf{R}_2)/k_B T_2] \cong C_{12} \exp[-U(\mathbf{R}_1)/k_B T_1] \tag{3.9}$$

where C_{12} is constant that depends on the state points.

Entropic invariance definition

Another and more formal way of defining isomorphs are through their invariance of configurational or excess entropy. Recall that the entropy of a system can be written as the sum of the ideal-gas entropy at the same density and temperature and an excess entropy $S = S_{\text{id}} + S_{\text{ex}}$ where S_{ex} necessarily is negative since the ideal gas must be more disordered than the liquid at the same density and temperature. The invariance of the excess entropy on isomorphs have been know from the original derivation, but here becomes the defining quantity.

A system is Roskilde-simple if the following relation holds for all physically relevant configurations

$$U(\mathbf{R}_a) < U(\mathbf{R}_b) \Leftrightarrow U(\lambda \mathbf{R}_a) < U(\lambda \mathbf{R}_b) \tag{3.10}$$

where $\mathbf{R}_a$ and $\mathbf{R}_b$ are micro configurations at the same state point and λ is a scaling factor [52]. To prove that this implies a constant constant excess entropy for Roskilde systems we define an instantaneous microscopical excess entropy $S_{\text{ex}}(\mathbf{R})$ as a function of the instantaneous potential energy $U(\mathbf{R})$ by letting the instantaneous excess entropy be equal to the thermodynamic excess entropy of a system with average potential energy equal to $U(\mathbf{R})$ and at the same density, ρ, as the configuration $\mathbf{R}$ [52]

$$S_{\text{ex}}(\mathbf{R}) \equiv S_{\text{ex}}(\rho, U(\mathbf{R})) \tag{3.11}$$

By inverting this formulation we get the instantaneous potential energy as function of the instantaneous excess entropy in the same manner as above

$$U(\mathbf{R}) = U(\rho, S_{\text{ex}}(\mathbf{R})) \tag{3.12}$$

assuming that equation (3.11) is bijective.

The above expressions for excess entropy and potential energy are general and does not relate to Roskilde-simple systems. The aim is now to use equation (3.10) to show that for Roskilde-simple systems, the instantaneous excess entropy and instantaneous potential energy both depend only on the reduced coordinates, which would imply that these are conserved between state points, for Roskilde-simple systems. First we use the micro canonical definition of excess entropy [52]

$$S_{\text{ex}}(\rho, U)/k_B = -N \ln N + \ln(\text{Vol}\{\tilde{\mathbf{R}} | U(\rho^{-1/3}\tilde{\mathbf{R}}) < U\}) \tag{3.13}$$

where Vol means the volume in the reduced coordinate configurational space.

With this we can write

$$S_{\text{ex}}(\mathbf{R}_1)/k_B = -N \ln N + \ln(\text{Vol}\{\tilde{\mathbf{R}} | U(\rho_1^{-1/3}\tilde{\mathbf{R}}) < U(\mathbf{R}_1)\}) \tag{3.14}$$

and

$$S_{\text{ex}}(\mathbf{R}_2)/k_B = -N \ln N + \ln(\text{Vol}\{\tilde{\mathbf{R}} | U(\rho_2^{-1/3}\tilde{\mathbf{R}}) < U(\mathbf{R}_2)\}) \tag{3.15}$$

but for Roskilde-simple systems we can use equation (3.10) to rewrite for instance equation (3.14) by multiplying both the potential energies that define the set with $\lambda = \rho_2^{-1/3}\rho_1^{1/3}$ to get

$$\begin{aligned} S_{\text{ex}}(\mathbf{R}_1)/k_B =& -N \ln N + \ln(\text{Vol}\{\tilde{\mathbf{R}} | U(\rho_2^{-1/3}\rho_1^{1/3}\rho_1^{-1/3}\tilde{\mathbf{R}}) < U(\rho_2^{-1/3}\rho_1^{1/3}\mathbf{R}_1)\}) \\ =& -N \ln N + \ln(\text{Vol}\{\tilde{\mathbf{R}} | U(\rho_2^{-1/3}\tilde{\mathbf{R}}) < U(\mathbf{R}_2)\}) \end{aligned} \tag{3.16}$$

which is the same as (3.15) for the entropy at the other state point, showing that the excess entropy only depend on the reduced coordinates [52]

$$S_{\text{ex}}(\mathbf{R}) = S_{\text{ex}}(\tilde{\mathbf{R}}) \tag{3.17}$$

and in turn equation (3.12) becomes [52]

$$U(\mathbf{R}) = U(\rho, S_{\text{ex}}(\tilde{\mathbf{R}})) \tag{3.18}$$

From this it is possible to derive some of the characteristic isomorph predictions. First we can derive the proportionality between Boltzmann factors found in equation (3.9) from a first order expansion of (3.18) around the thermodynamic excess entropy at constant density

$$U(\mathbf{R}) \approx U + \left(\frac{\partial U(\mathbf{R})}{\partial S_{\text{ex}}(\mathbf{R})}\right)_\rho (S_{\text{ex}}(\tilde{\mathbf{R}}) - S_{\text{ex}}) \tag{3.19}$$

$$\approx U + T(\rho, S_{\text{ex}})(S_{\text{ex}}(\tilde{\mathbf{R}}) - S_{\text{ex}}) \tag{3.20}$$

where S_{ex} is short hand for the thermodynamic excess entropy and U for the average potential energy. If we pick two state points with the same excess entropy S_{ex}, $(\rho_1, T_1 = T(\rho_1, S_{\text{ex}}))$ and $(\rho_2, T_2 = T(\rho_2, S_{\text{ex}}))$, and for these state points pick two micro configurations with the same reduced coordinates $\mathbf{R}_1$ and $\mathbf{R}_2$ equation (3.20) implies that

$$S_{\text{ex}}(\tilde{\mathbf{R}}) - S_{\text{ex}} \approx \frac{U(\mathbf{R}_1) - U_1}{T_1} \approx \frac{U(\mathbf{R}_2) - U_2}{T_2} \tag{3.21}$$

giving the wanted relation.

As pointed out, the two ways of defining the isomorph criteria are equivalent. To see this, we again pick a set of state points (ρ_1, T_1) and (ρ_2, T_2), with the same excess entropy. This makes them isomorphic in the latter sense, and the aim is now to show, that this also makes them isomorphic in the former sense by deriving an expression for $U(\mathbf{R}_2)$ of the same form as the one in (3.4). We pick two micro configurations $\mathbf{R}_1$ and $\mathbf{R}_2$ with the same reduced coordinates. By combining equations (3.11) and (3.12) we have

$$\begin{aligned} U(\mathbf{R}_1) =& U(\rho_1, S_{\text{ex}}(\rho_1, U(\mathbf{R}_1))) \\ U(\mathbf{R}_2) =& U(\rho_2, S_{\text{ex}}(\rho_2, U(\mathbf{R}_2))) \end{aligned} \tag{3.22}$$

but since from equation (3.17) we know that S_{ex} is a function of the reduced coordinates, for Roskilde simple systems, we get

$$S_{\text{ex}}(\rho_1, U(\mathbf{R}_1)) = S_{\text{ex}}(\rho_2, U(\mathbf{R}_2)) \tag{3.23}$$

which means, that we can write $U(\mathbf{R}_2)$ as

$$U(\mathbf{R}_2) = U(\rho_2, S_{\text{ex}}(\rho_1, U(\mathbf{R}_1))) \tag{3.24}$$

which is what we wanted to show when one identifies f_1 of equation (3.4) with

$$f_1(\rho_2, U(\mathbf{R}_1)) = U(\rho_2, S_{\text{ex}}(\rho_1, U(\mathbf{R}_1))) \tag{3.25}$$

Further more we can see from this definition of f_1 is consistent with our choice of temperatures in equations (3.6) and (3.7), where we chose

$$T_2 = \left(\frac{\partial f_1(\rho_2, U(\mathbf{R}_1))}{\partial U(\mathbf{R}_1)} \right)_{\rho_1, \rho_2} T_1 \tag{3.26}$$

in order to get isomorphic state points, since

$$\left(\frac{\partial f_1}{\partial U(\mathbf{R}_1)} \right)_{\rho_1, \rho_2} = \left(\frac{\partial U(\rho_2, S_{\text{ex}}(\rho_1, U(\mathbf{R}_1)))}{\partial U(\mathbf{R}_1)} \right)_{\rho_1, \rho_2} \tag{3.27}$$

$$= \left(\frac{\partial U(\mathbf{R}_2)}{\partial S_{\text{ex}}} \frac{\partial S_{\text{ex}}}{\partial U(\mathbf{R}_1)} \right)_{\rho_1, \rho_2} \tag{3.28}$$

$$= \frac{T_2}{T_1} \tag{3.29}$$

This implies that the two way of defining isomorphs are consistent. Though the above derivations have related pairs of state points, it follows immediately, that if state points 3 is isomorph to state points 1 it is also isomorph to state points 2, making being isomorphic an equivalence relation. This, together with the fact that the density changes between isomorphic state points can be made arbitrarily small means, that it is possible to map out lines in the ρ, T-phase plane, along which all state points are isomorphic to one another. These lines are called isomorphs.

3.4 Isomorph properties

Though a lot of measurable quantities are invariant on isomorphs, there are really three main invariances on isomorphs:

- Invariance of canonical probabilities of micro configurations with the same reduced coordinates.
- Invariance of the reduced at micro configurations with the same reduced coordinates.
- Invariance of excess entropy of the isomorphic state points.

Invariance of reduced probabilities

From equation (3.9) it is given that for any relevant pair of micro configurations with the same reduced coordinates, we have proportional Boltzmann factors. Using this we can write the probabilities of the reduced micro configuration at the different state points as

$$P(\rho_2^{-1/3}\tilde{\mathbf{R}}_2)Z_2 \approxeq C_{12}P(\rho_1^{-1/3}\tilde{\mathbf{R}}_1)Z_1 \tag{3.30}$$

where C_{12} is the state point dependent proportionality constant, but the partition function Z is just an integral over Boltzmann factors giving

$$Z_2 \approxeq \frac{1}{C_{12}}Z_1 \tag{3.31}$$

showing that the canonical probabilities are invariant to a good approximation on the isomorph [23].

Invariance of reduced forces

The reduced force is given by

$$\tilde{\mathbf{F}}(\mathbf{R}) = \frac{\mathbf{F}(\mathbf{R})}{\rho^{1/3}k_BT} \tag{3.32}$$

From equation (3.4) we have

$$U(\mathbf{R}_2) \approxeq f_1(\rho_2, U(\mathbf{R}_1)) \tag{3.33}$$

Since the force $F(\mathbf{R})$ is the negative gradient of U we get

$$-\nabla_{\tilde{\mathbf{R}}}U(\mathbf{R}_2) \approxeq -\nabla_{\tilde{\mathbf{R}}}f_1(\rho_2, U(\mathbf{R}_1)) \tag{3.34}$$

$$-\rho_2^{-1/3}\nabla_{\mathbf{R}_2}U(\mathbf{R}_2) \approxeq -\left(\frac{\partial f_1(\rho_2, U(\mathbf{R}_1))}{\partial U(\mathbf{R}_1)}\right)_{\rho_2}\rho_1^{-1/3}\nabla_{\mathbf{R}_1}U(\mathbf{R}_1) \tag{3.35}$$

$$\rho_2^{-1/3}\mathbf{F}(\mathbf{R}_2) \approxeq \rho_1^{-1/3}\mathbf{F}(\mathbf{R}_1)\left(\frac{\partial f_1(\rho_2, U(\mathbf{R}_1))}{\partial U(\mathbf{R}_1)}\right)_{\rho_2} \tag{3.36}$$

and if we pick our temperatures, like above, as

$$\left(\frac{\partial f_1(\rho_2, U(\mathbf{R}_1))}{\partial U(\mathbf{R}_1)}\right)_{\rho_2} = \frac{T_2}{T_1} \tag{3.37}$$

we get for the forces

$$\rho_2^{-1/3}\mathbf{F}(\mathbf{R}_2) \approxeq \rho_1^{-1/3}\mathbf{F}(\mathbf{R}_1)\frac{T_2}{T_1} \tag{3.38}$$

$$\tilde{\mathbf{F}}(\mathbf{R}_2) \approxeq \tilde{\mathbf{F}}(\mathbf{R}_1) \tag{3.39}$$

Invariance of the excess entropy

This invariance follows immediately from the second definition of isomorphs where it is the defining criteria, but can also be derived from the invariance of probability distributions, since excess entropy in the canonical ensemble can be written as [23]

$$S_{\text{ex}} = k_B \int d\tilde{\mathbf{R}} P(\tilde{\mathbf{R}}) \ln P(\tilde{\mathbf{R}}) \tag{3.40}$$

As a side note it is worth mentioning that since the isomorph theory predicts an invariance of dynamics on the lines of constant excess entropy, this is in agreement with the Roselfeld's excess entropy scaling [18, 47].

3.5 Finding isomorphs

There are several different ways of finding isomorphs but there are two prominent methods. The first is related to the invariance of the excess entropy and the second to the scaling of the energy landscape.

Isomorphs from excess entropy

Writing the excess entropy as a function of volume and temperature, $S_{\text{ex}} = S_{\text{ex}}(V, T)$ we can write up the full derivative of S_{ex} as

$$dS_{\text{ex}} = \left(\frac{\partial S_{\text{ex}}}{\partial V}\right)_T dV + \left(\frac{\partial S_{\text{ex}}}{\partial T}\right)_V dT \tag{3.41}$$

Setting this to zero will map out curves in (V, T)-space of constant excess entropy

$$dS_{\text{ex}} = 0 \tag{3.42}$$

$$\left(\frac{\partial S_{\text{ex}}}{\partial V}\right)_T dV = -\left(\frac{\partial S_{\text{ex}}}{\partial T}\right)_V dT \tag{3.43}$$

Using Maxwell's relations for configurational quantities this can be rewritten as [23]

$$\left(\frac{\partial S_{\text{ex}}}{\partial V}\right)_T dV = -\left(\frac{\partial S_{\text{ex}}}{\partial T}\right)_V dT \tag{3.44}$$

$$\frac{1}{V}\left(\frac{\partial W}{\partial T}\right)_V dV = -\left(\frac{\partial S_{\text{ex}}}{\partial U}\right)_V C_v dT \tag{3.45}$$

$$\frac{\langle \Delta U \Delta W \rangle}{k_B T^2} d\ln V = \frac{1}{T}\frac{\langle (\Delta U)^2 \rangle}{k_B T^2} dT \tag{3.46}$$

$$\left(\frac{d\ln T}{d\ln \rho}\right)_{S_{\text{ex}}} = \frac{\langle \Delta U \Delta W \rangle}{\langle (\Delta U)^2 \rangle} \tag{3.47}$$

where W is the virial, see equation (3.1).

From this it is possible to see that in order to map out lines of constant excess entropy, a small change λ in density can be compensated by a change in temperature as

$$S_{\text{ex}}(\rho, T) = S_{\text{ex}}((1+\lambda)\rho, (1+\lambda\gamma)T) \tag{3.48}$$

where γ is a scaling exponent given by

$$\gamma \equiv \left(\frac{\partial \ln T}{\partial \ln \rho}\right)_{S_{\text{ex}}} = \frac{\langle \Delta U \Delta W \rangle}{\langle (\Delta U)^2 \rangle} \tag{3.49}$$

which can be calculated from a simulation as the slope of a linear regression fit to the potential energy-virial data, i.e. $U(\mathbf{R}), W(\mathbf{R})$.

So in order to find isomorphs, one can map out the configurational adiabat by simulating at an initial state point ρ_0, T_0 and calculating the scaling exponent γ. Then for a small change in density, the corresponding change in temperature is know, and one has a new state point ρ_1, T_1 and the procedure can then be repeated using the new state point as reference.

Equations (3.48) and (3.49) are general, and can be used to map out the lines of constant excess entropy, regardless of whether the system have isomorphs, so in order to find out if a system have isomorphs, one would in principle have to test the invariance of one of the isomorphic quantities. One way of estimating whether a system will have isomorphs, before performing simulations at the new density and temperature, is to look at the correlation coefficient R. As a guide, only strongly correlating systems have isomorphs, though isomorphs have been found in complex systems with a correlation coefficient of $R = 0.86$ [65] underlining that the limit $R > 0.9$ is somewhat arbitrary. None the less, isomorphic behaviour does require a numerically high correlation coefficient [4, 23, 52].

Since this method relies on a first order differentiation of the excess entropy it does not allow for very large changes in state point, usually no greater than a couple of percentage change in density. The next method is more flexible in this respect

Direct isomorph check

This method relies on the scaling properties of the energy landscape. From the first order Taylor expansion of equation (3.4) and using the relation of equation (3.6) we had

$$U(\mathbf{R}_2) \approxeq \frac{T_2}{T_1} U(\mathbf{R}_1) + g_1(\rho_2) \tag{3.50}$$

In order to utilize this, one can perform a simulation at ρ_1, T_1 and calculating what the potential energy at density ρ_2 would be, for the micro configurations of the simulation by calculating $U_2 = U(\rho_2^{-1/3}\rho_1^{1/3}\mathbf{R}_1)$ as was shown on figure 3.1.

According to equation (3.50) the energies $U_1 = U(\mathbf{R}_1)$ and U_2 should be linearly dependent, with a proportionality given by T_2/T_1 so by finding the slope of the U_1, U_2-plot, the temperature T_2 can be found and this temperature should then give an isomorphic state points ρ_2, T_2 to the reference state point ρ_1, T_1.

The possible size density steps allowed by this method are larger than those the mapping of configurational adiabats. The method does have a computational challenge in that the potential energy need to be calculated at two different densities simultaneously.

Having introduced the basic principles of isomorph theory we continue by showing how it has been applied in systems of simple crystal solids to predict invariances of those.

4 Roskilde crystals

In this chapter we apply the isomorph theory to a number of crystalline systems. While the theory is in principle developed to describe the liquid behaviour it turns out that it works as well if not better for solids. The result presented here where published in the paper [1]. Some of the work was done as part of a masters thesis [38].

In the previous chapter, the isomorph theory was introduced, and shown to be an explanation for the existence of empirical density scaling found for a large class of liquids systems.

While the isomorph theory was in principle developed to describe liquid systems it could be of interest to see if it applies equally well or even better for crystalline systems.

We present in this chapter results for a series of crystalline systems, some of which have isomorphs to illustrate the theory, both application and limits. As such the chapter will not include extensive introduction to the crystal phase. We refer instead to the literature for a general introduction [3, 30].

The primary system studied is the single component Lennard-Jones system as a model for a general van der Walls crystal. All particles are of the same type, and the interactions are given by the very simple Lennard-Jones pair potential

$$v(r_{ij}) = 4\epsilon \left[\left(\frac{\sigma}{r_{ij}} \right)^{12} - \left(\frac{\sigma}{r_{ij}} \right)^{6} \right] \tag{4.1}$$

with parameters $\epsilon = \sigma = 1.0$. The particles where set up in a perfect $10 \times 10 \times 10$ face centered cubic (fcc) lattice. While the Lennard-Jones crystal does energetically favor the hexagonal close packed (hcp) structure, the difference in free energies of the two structures is so low ($\sim 0.01\%$), that the fcc lattice can be considered a stable structure [61]. This structure also have the added advantage that it fits in cubic periodic boundary conditions.

In the following we investigate the single component Lennard-Jones (LJ) crystal in the crystal phase, showing that it obeys the criteria for strong correlation and that the state points found using the direct isomorph check gives invariant behavior. In particular, the radial distribution function $g(r)$ will be used to measure invariance of the structure. It is a measure of the structure of the system, normalized by a completely random system, and is a classic measure of structure in liquids [26]. For crystal systems each crystal structure has a signature form of the radial distribution

function. As many of the following systems are simulated in fcc crystal structures their radial distribution function will look similar.

4.1 Strongly correlating crystals

Following the idea for strongly correlating liquids, we look here at the correlation between the fluctuations in instantaneous potential energy U and virial W. The top panel of figure 4.1 shows the normalized fluctuations in potential energy and virial as a function of time, for a simulation of the LJ crystal. The two values follow each other perfectly and by calculating the correlation using equation 3.2 one gets the value $R = 0.999$. This is clearly a strongly correlating system. To test whether this is a feature of the particular LJ crystal or of crystals in general we introduce a new model, a model referred to here as the NaCl since it derives from a model of liquid NaCl [55] and is a simple binary ionic model. The interactions of this model are given by a Lennard-Jones potential with an added Coulomb potential

$$v_{ij}(r_{ij}) = 4\epsilon_{ij}\left[\left(\frac{\sigma_{ij}}{r_{ij}}\right)^{12} - \left(\frac{\sigma_{ij}}{r_{ij}}\right)^{6}\right] + \frac{z_i z_j e^2}{4\pi\epsilon_0 r_{ij}} \tag{4.2}$$

where ϵ_{ij}, σ_{ij} and z_{ij} depend on the type of the interacting particles. Details on the parameters can be found in [55]. To deal with the long-range interactions of the Coulomb potential, shifted force-cut off where used, with a $R_c = 6.5\rho^{-1/3}$, shown to work well for Coulomb interactions [25]. This system was simulated as two interpenetrated fcc cubic lattices, consisting of one particle type each, the structure of ordinary NaCl crystals [30]. Due to the added ionic interactions we do not expect this system to be strongly correlating and consequently we expect it to have isomorphs, since it will not have isomorphs in the liquid phase. The correlation for this model is also included as the bottom panel of figure 4.1 and while the correlation $R = 0.828$ shows that the system is not a strongly correlating one, it is not far from the limit, and as was mentioned, isomorphs have been found is systems with $R = 0.86$ [65], so it is not impossible that this system will have isomorphs.

We test this by using the direct isomorph check to find state points that should be isomorphic, and test for invariance of structure and dynamics.

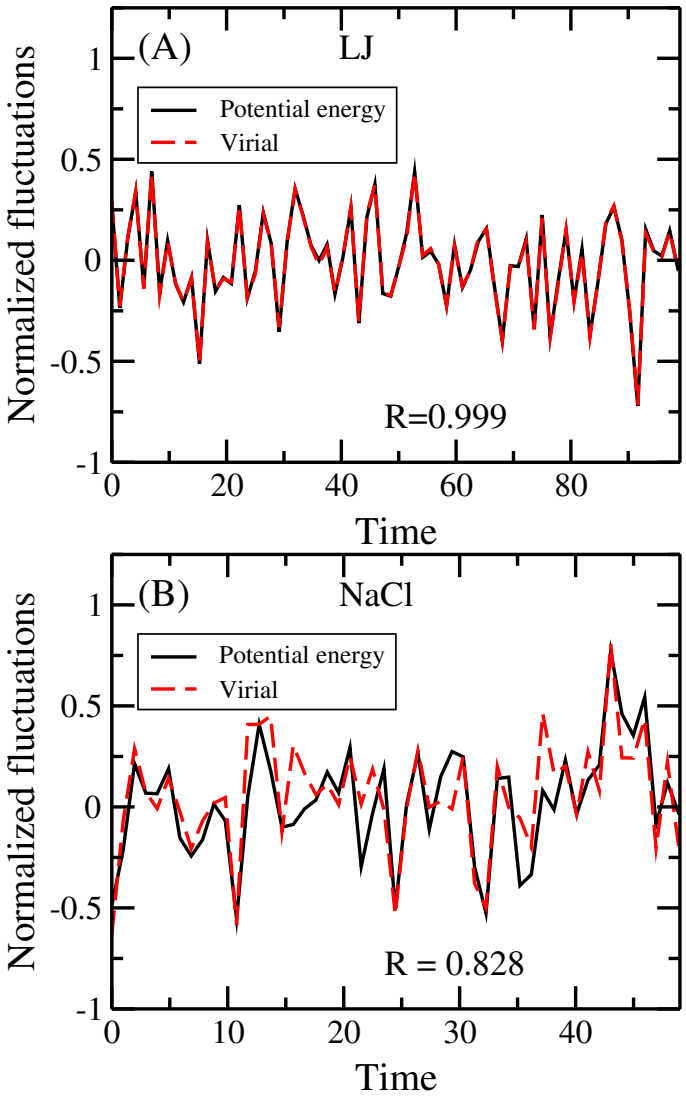

Figure 4.1: The fluctuations in potential energy and virial for the Lennard-Jones crystal, (A), and the NaCl model, (B). With $R_{LJ} = 0.999$ for the Lennard-Jones crystal we expect the Lennard-Jones crystal to have isomorphs. For the NaCl model $R_{NaCl} = 0.828$ which is below the limit for a strongly correlating liquid, but not too far so the NaCl model might have isomorphs. Reproduced from [1].

4.2 Finding isomorphic state points

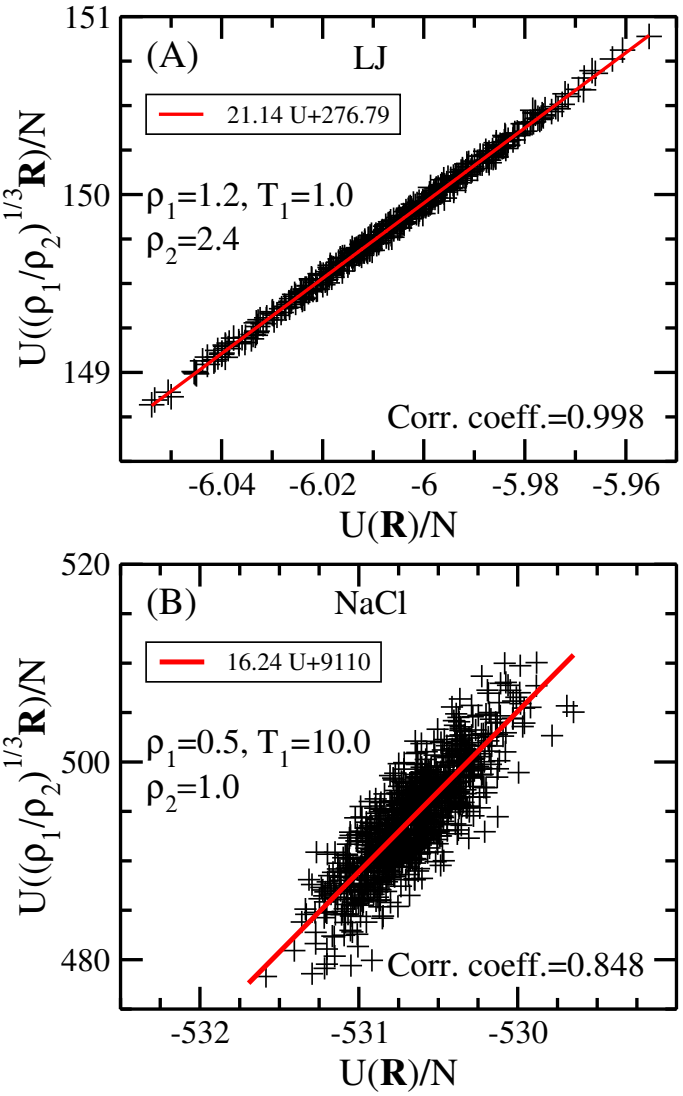

Figure 4.2: The scaled and unscaled potential energy for the Lennard-Jones, (A), and NaCl model, (B). In both cases the scaled density is twice the unscaled one. Using the slope of a linear regression to the data, one can find the relation temperature T_2/T_1, where T_2 should give isomorphic behaviour, given that the system have isomorphs. Reproduced from [1].

While it is possible to map out the isomorphs as configurational adiabats we find isomorphs here from the direct isomorph check as introduced in the previous chapter,

see 3.5. By comparing the potential energy at two micro configurations with the same reduced coordinates at different densities, ρ_1 and ρ_2, one can get the relationship $h(\rho_2/\rho_1) = T_2/T_1$, which from the reference state point (ρ_1, T_1) makes it possible to calculate the temperature T_2 that makes the state point (ρ_2, T_2) isomorphic to the reference state point. An illustration of the procedure is shown on figure 4.2 for both the LJ model, top panel, and the NaCl model, bottom panel. In both cases the potential energy of unscaled and scaled configurations are plotted against each other, and the resulting scatter data is fitted by a straight line. The slope then gives the wanted relation. In case of the LJ crystal one gets for the reference state point $(\rho_1, T_1) = (1.2, 1.0)$ and $\rho_2 = 2\rho_1 = 2.4$, that the temperature $T_2 = 21.14\, T_1 = 21.14$ should give invariant reduced dynamics and structure if the system have isomorphs. Likewise for the NaCl model, the state point $(\rho_2, T_2) = (1.0, 162.4)$ should give invariant behaviour to the reference state point $(\rho_1, T_1) = (0.5, 10)$.

4.3 Structural invariance

To test whether the systems have isomorphs we compute the radial distribution function for the two model systems at state points found with this method to test for invariance. For the LJ model the result of these calculations can be seen on the top panel of figure 4.3. Though not very clear on the figure, there are in fact seven different state point, plotted on top of each other. The collapse of the structure is extra ordinary, even for systems with isomorphs. To test whether this invariance is simply due to qualities of the LJ crystal and not isomorphs, figure 4.3 also includes data for the radial distribution function calculated along an isotherm. Here there are no collapse showing that the invariance of the structure is not a general feature of the LJ crystal. Likewise, state points along an isochore were simulated and tested for collapse in both structure and dynamics and no collapse was found. At a large number of these state points, the systems melted. That data is not presented here, but may be found in the paper [1].

For the NaCl the result is quite different. Figure 4.4 shows the radial distribution function for a set of state points found with the direct isomorphs check. Each panel shows the calculations carried out over a set of pair types, e.g. the top panel shows the radial distribution function for particles of different types. In none of the cases are there any significant collapse of the data. That the data seems to collapse in the minimas is a result of the fact that when calculated in reduced units, the crystal structure results in minimas at certain distances. For the highest density $\rho = 0.9$, the system is melted giving a structure completely different from the others.

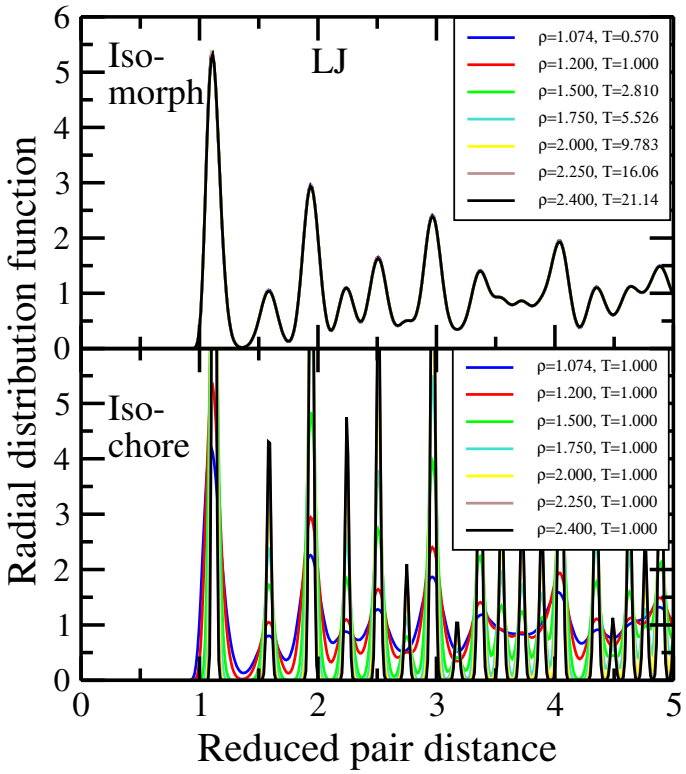

Figure 4.3: The radial distribution function along the isomorph for the Lennard-Jones crystal as a function of reduced pair distance. The collapse are impressive, even for isomorphic systems. Also included is the radial distribution function of the system along an isotherm to show that the collapse is not an inherent feature of the LJ fcc crystal system. Reproduced from [1].

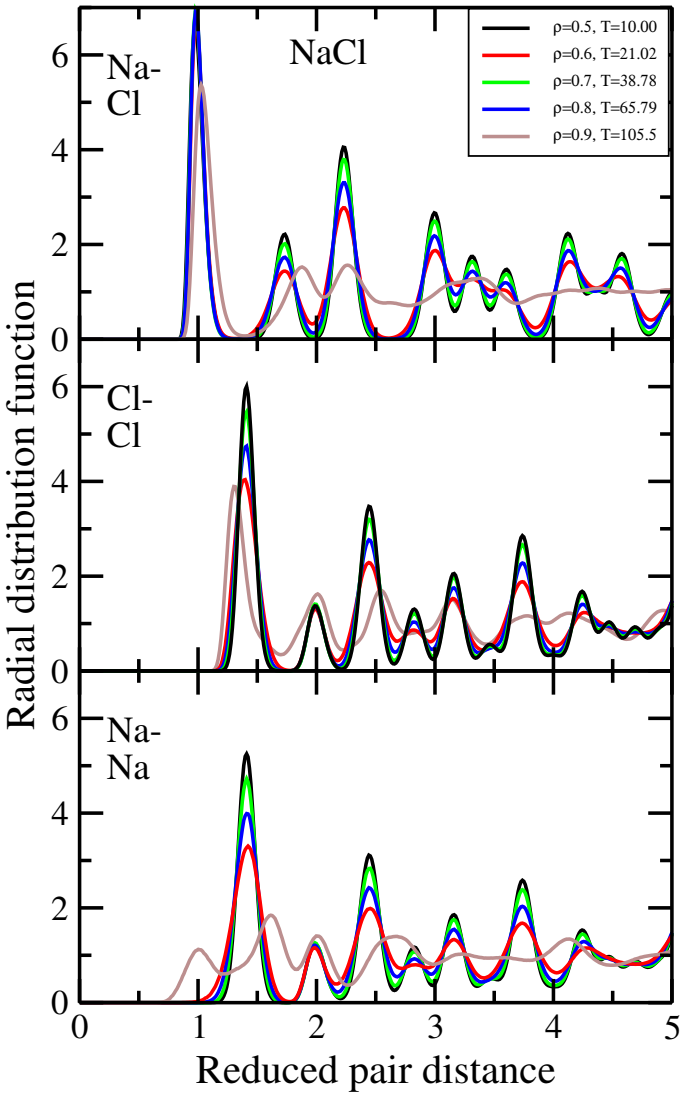

Figure 4.4: The radial distribution function along a set of state points generated by the direct isomorph check for the NaCl model. Each panel corresponds to the pair distance of a set of types. Here, as expected, there are no collapse showing that the NaCl model does not have isomorphs in the crystal phase. Reproduced from [1].

4.4 Dynamical invariance

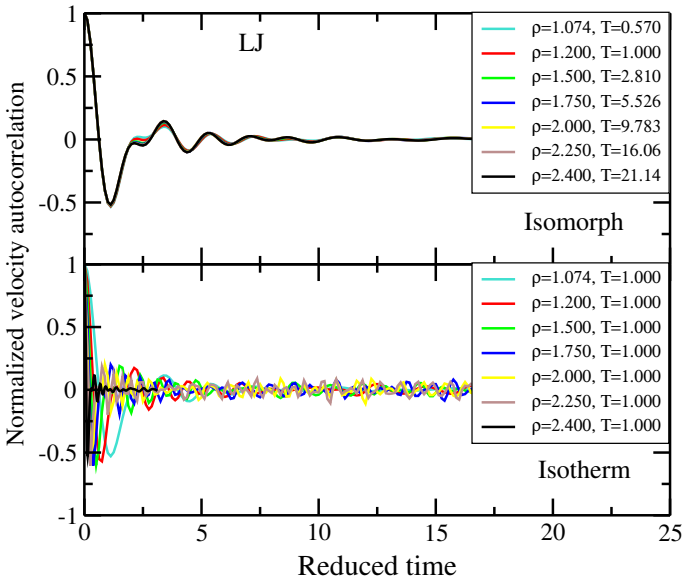

Figure 4.5: The normalized velocity autocorrelation function as a function of the reduced time for the Lennard-Jones crystal along the isomorph and an isotherm. As a measure of dynamics, this figure shows that the isomorphic behaviour of the crystal also includes invariance of dynamics and that the isotherm does not exhibit such an invariance. Reproduced from [1].

Besides structure, the isomorph theory predicts that the dynamics are invariant along an isomorph. In liquids this is usually shown with the collapse of the long time dynamics, for instance via the diffusion of the system. In a perfect crystal such as the one used here, there are no real long time dynamics. Instead we calculate the normalized velocity self autocorrelation

$$A_v(t) = \frac{\langle \mathbf{v}_i(t) \cdot \mathbf{v}_i(0) \rangle}{\langle \mathbf{v}_i(0) \cdot \mathbf{v}_i(0) \rangle} \tag{4.3}$$

where the mean $\langle \cdot \rangle$ is taken both over particles and initial times $t = 0$. For the LJ crystal this was calculated along the isomorph and the isotherm. Figure 4.5 shows these data, and the collapse of the data for the isomorphic state points further confirms that the isomorph theory applies for the crystal phase.

Another way of probing dynamics of the crystal phase is to introduce defects. We introduced eight vacancies in a perfect $8 \times 8 \times 8$ LJ crystal giving a vacancy density of $\rho_{\text{vac}} = 0.004$. This will introduce some lattice jumping on a time scale much slower than that probed by the velocity autocorrelation. We measured the mean square displacement,

$$\text{msd}(t) \equiv \langle (\mathbf{r}_i(t) - \mathbf{r}_i(0))^2 \rangle \tag{4.4}$$

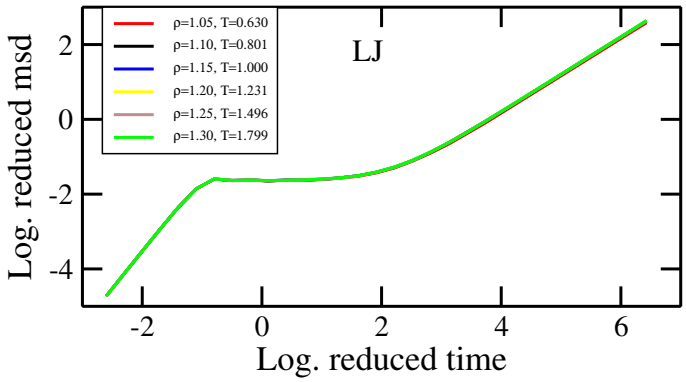

Figure 4.6: Diffusion in Lennard-Jones crystals with a small number of vacancies. Note that this is the total mean square displacement of the system. Also this measure of long time dynamics collapses even though the configurations related to the diffusion of a particle only constitutes a very small volume of the entire configurational space. Reproduced from [1].

over large time intervals in such a defect crystal for several isomorphic state points, shown in figure 4.6.

The data shown is for the total mean square displacement so also the particles far from the vacancies are included in the mean, e.g. a msd-value of 1 corresponds to all particles having moved one interparticle distance on average.

From the collapse it is clear that also the long time dynamics of a defect crystal can be predicted by the isomorph theory despite the fact that the configurations corresponding to a lattice jumps represent only a very small fraction of the entire available configurational space.

4.5 Isomorph jumps

Another classic test of isomorph theory is the isomorph jump [23]. Owing to the invariance between isomorphic state points of the probabilities for micro configurations with the same reduced coordinates, it follows that any equilibrium configuration taken from one state points can be scaled to a different state point isomorphic to the first, and still be an equilibrium configuration. This is tested for the LJ crystal by instantaneously changing the density and/or temperature of a micro configuration, and measuring the relaxation through the potential energy of the system. On figure 4.7 this is done for the three different jump types; an isomorphic, an isochoric and an isothermal jump. While all systems show fast relaxation, the relaxation is fastest for the isomorphic jump despite this being the greatest jump measured in (ρ, T)-space.

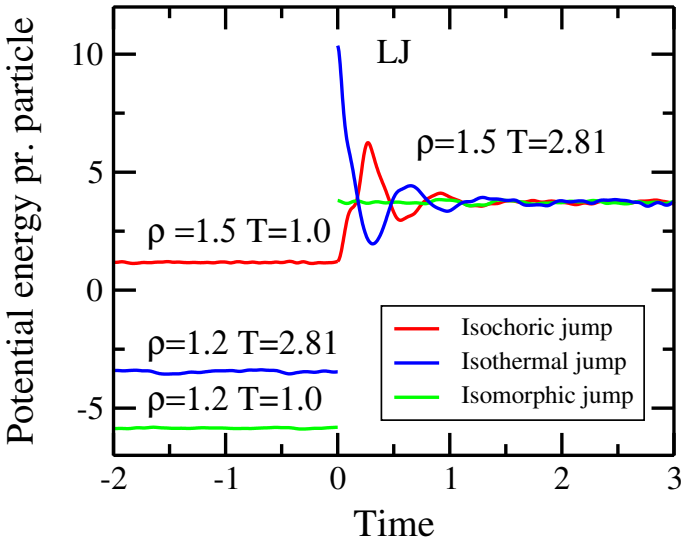

Figure 4.7: The relaxation of the Lennard-Jones crystal after an instantaneous change in temperature and/or volume. Of the three jumps the isomorphic jump is the greater one measured in (ρ, T)-space but has the shortest relaxation time. Reproduced from [1].

4.6 Other crystalline systems

To broaden the investigation and test whether there might be another explanation for the fact that the data from the NaCl model do not scale, other than that the model does not have isomorphs, we test a series of other crystalline systems. Each system is picked to test a specific point. The reasoning is explained in greater detail in the paper [1]. The procedure of mapping out isotherms and isochores to show that it is in fact only the isomorphic state points that have invariance was repeated for a number of the following systems, confirming this. That data is not presented here, but can be found in the paper.

First we test whether it is simply the fcc crystal structure that gives the isomorphic behaviour of the LJ crystal. To this end we simulate the Wahnström binary Lennard-Jones system [69], which crystallizes in a Laves phase [41], a crystal phase with twelve atoms in the unit cell. As the name suggest, the model consists of two particle types, in a 50/50-mixture, interacting via the Lennard-Jones potential. The parameters can be found in [69]. Shown on figure 4.8 is the all-particle radial distribution function calculated for two state points, found with the direct isomorph check. Again the collapse is impressive even by isomorph standards. The figure confirms, that it is not the particular crystal phase, that gives rise to the isomorphic behavior.

Secondly we investigate whether it is only the Lennard-Jones potential or perhaps a potential that is the sum of inverse power law (IPL) terms that can give isomorphic crystals. To test this we use the Buckingham potential [11]

$$v(r) = \epsilon \left(\frac{6}{\alpha - 6} \exp[\alpha(1 - r/\sigma)] - \frac{\alpha}{\alpha - 6} \left(\frac{r}{\sigma} \right)^{-6} \right) \tag{4.5}$$

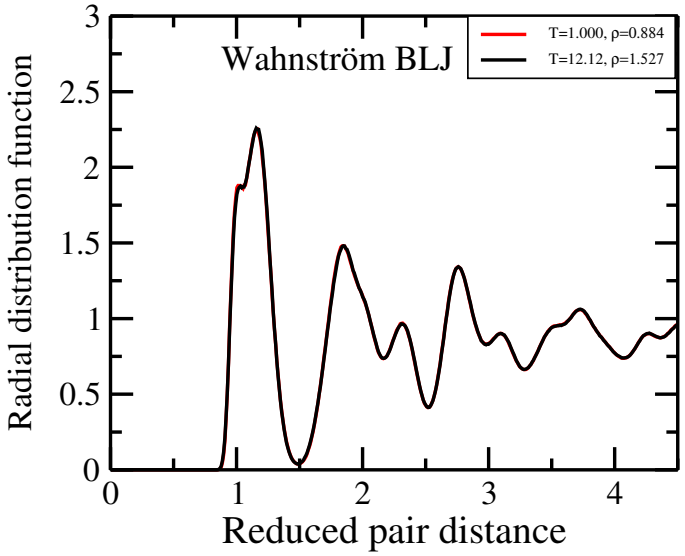

Figure 4.8: All-particle radial distribution of the Wahnström binary Lennard-Jones model. This model forms a complex Laves crystal structure. Despite this, the model also have isomorphs. Reproduces from [1].

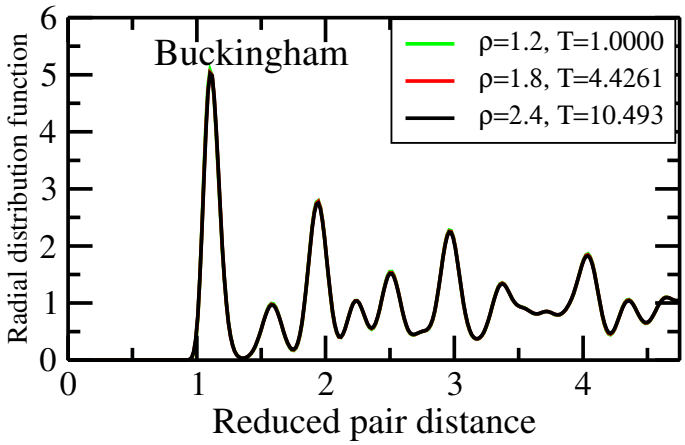

Figure 4.9: The radial distribution function of the Buckingham potential. The Buckingham potential differs greatly from the Lennard-Jones potential, showing that it is not the pure Lennard-Jones potential that allows for isomorphic behavior.

This potential is quite different from the Lennard-Jones potential, but liquid systems interacting with the Buckingham potential have been shown to have isomorphs [63]. Setting up a fcc crystal of particles interacting via the Buckingham potential, finding three isomorphic state points and calculating the radial distribution function for these results in the data presented on figure 4.9. Also here the collapse of the data is very close to perfect, showing that it is not only Lennard-Jones potentials that have isomorphs in the crystal phase.

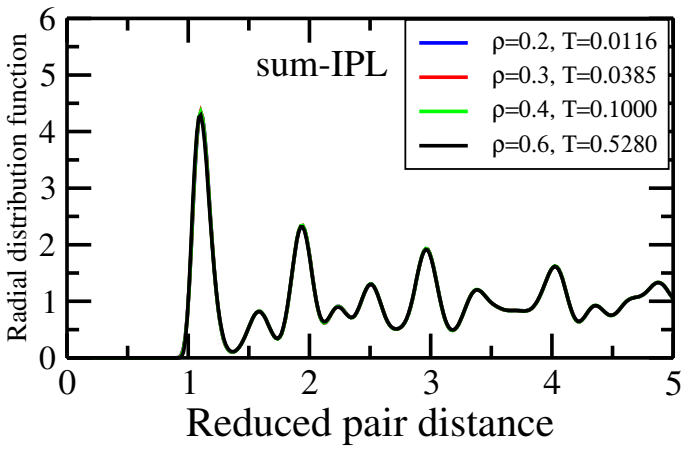

Figure 4.10: The radial distribution function of the "sum-IPL" model. Despite the hard core of the potential, the system have isomorphs as shown from the invariance of the structure. Reproduces from [1].

While a potential consisting of a single IPL term trivially obeys isomorph theory [23] it could be, that it is the number of IPL terms that prevents the NaCl system showing invariance. To test this hypothesis we simulated a crystal with a potential referred to here as the "sum-IPL" system, since it is the integral over all IPL terms with an exponent greater than some n_0

$$v(r) = \epsilon \int_{n_0}^{\infty} dn (r/\sigma)^{-n} \tag{4.6}$$

$$= \epsilon \frac{(r/\sigma)^{-n_0}}{\ln(r/\sigma)} \quad (r > \sigma) \tag{4.7}$$

We simulated this potential with $n_0 = 6$ and with interparticle distances all greater that the distance of divergence $r = \sigma$. This system was also set up in an fcc lattice, and the radial distribution function calculated for isomorphic state points found with the direct isomorph check. In [64] it was shown that the model have isomorphs in the liquid phase, so we expect it to have isomorphs in the crystal phase as well, which is confirmed by the data presented in figure 4.10, showing data for three isomorphic state points.

With all these different model systems, it seems that the reason the NaCl crystal does not have isomorphs in the crystal phase is the same as the reason it does not have it in the liquids face, the strong long-ranged interactions of the Coulomb potential [5, 53]

We turn instead to a different class of model systems, molecular models. As mentioned, the isomorph theory have been tested for a number of molecular models, and we present here two such models simulated in the crystal phase. The first model

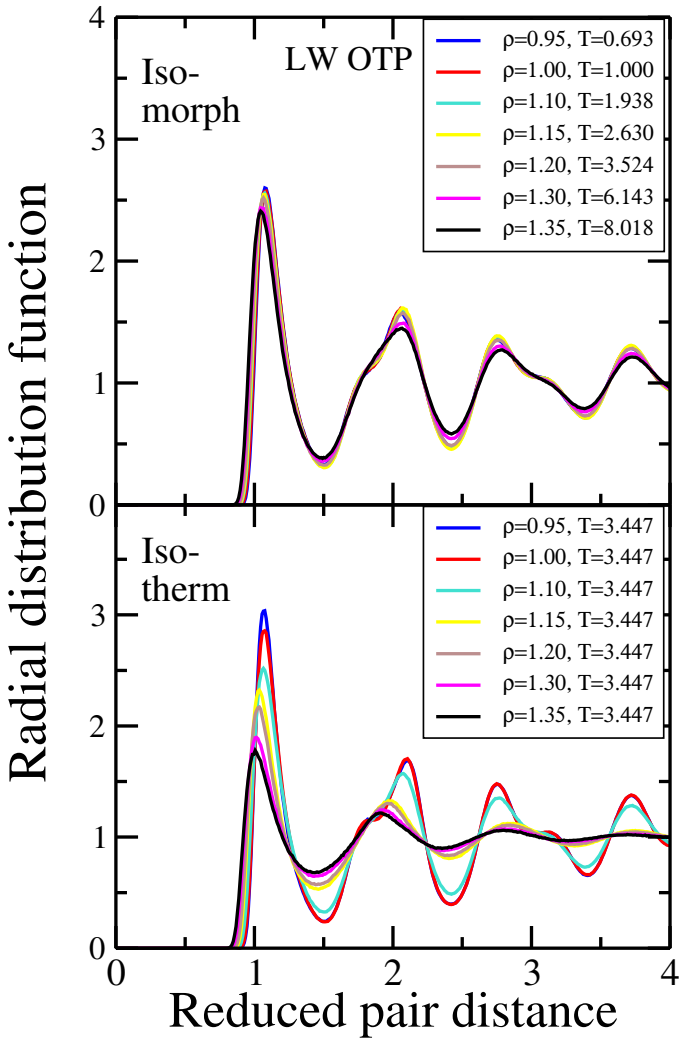

Figure 4.11: The intermolecular atom-atom radial distribution function calculated for the Lewis-Wahnström OTP model simulated on state points along an isomorph. The collapse is not as good as for the isomorphic atomic models, but still better than that found for the NaCl model. Also included is the radial distribution calculated along an isotherm to illustrate, that there is in fact a collapse of the isomorph data. Reproduced from [1].

is the Lewis-Wahnström ortho-terphenyl (OTP) model [35]. This model is a three particle molecular model, with each particle corresponding to a phenyl-group. The

particles interact with the Lennard-Jones potential and the intramolecular distances are fixed using constraints, with a 75° angle. The results for this model is shown in figure 4.11, and are less impressive than the corresponding results for the non-molecular systems with isomorphs. Still, comparing to the NaCl model the collapse is very clear. For this model we have also included the data for an isotherm. This was done to illustrate the difference between a not-perfect collapse, along the isomorph, and a non-existing one.

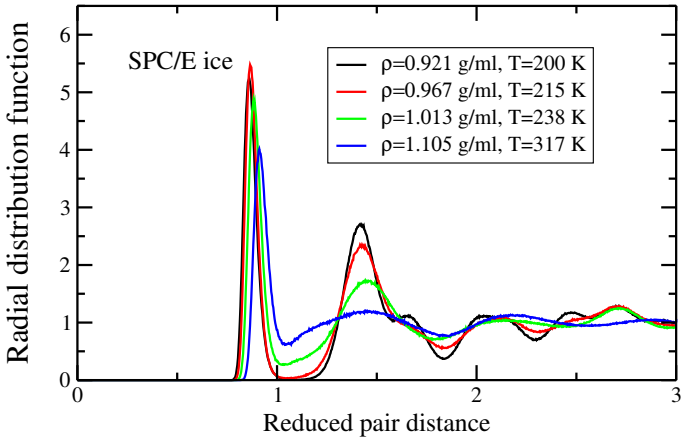

Figure 4.12: Ice, here modeled with the SPC/E hexagonal model, does not have isomorphs, as evident from the lack of collapse in the oxygen-oxygen radial distribution function. Water has generally been an example of a system with out isomorphs [23]. Like the NaCl model it has strong long-range interactions, greatly reducing the potential energy-viral correlation. Reproduced from [1]

Lastly we show data for simulations of ice, modeled with the three site SPC/E hexagonal model [9]. From the data presented in figure 4.12 it is clear that the model does not have isomorphs. Given that water has near zero potential energy-virial correlation and has been used as an example of a system without isomorphs [23], this further confirms the result, that the systems without isomorphs in the liquid phase does not have isomorphs in the crystal phase.

4.7 Summary

We have demonstrated how to apply the isomorph theory. By generating state points that should give invariant dynamics and structure and then testing for these invariances, it is often easy to determine whether a systems has isomorphs. One could imagine borderline cases, where it is hard to determine if a system has isomorphs, but for all systems tested here there are a clear distinction between systems with isomorphs and systems without.

Further more we have shown in this section that the isomorph theory work very well in the crystal phase, giving an even better collapse of structure and dynamics than isomorphs in the liquid phase. The reasons for this is still unknown. None the

less it stands, that having isomorphs is not a phase-related property, but survives the first order phase transition.

Part II

Pseudosomorphs

5 Pseudoisomorphs

This chapter deals with systems that behave like isomorphic systems but lack the defining feature of invariant excess entropy, so called *pseudo*isomorphic systems. We introduce the molecular models that are used in this thesis, and illustrates the behavior of systems with intramolecular springs.

5.1 Characterization

Though the isomorph theory is working very well in predicting the behaviour of a large class of model systems, including molecular models, there are some systems, for which it does not work. These include, as shown in the chapter 4, systems with Coulomb interactions, but also molecular models, where the bonded interactions are not a constraint.

In a recent paper [66] it was shown, that the Lennard-Jones chain with intramolecular harmonic springs does not have isomorphs. The authors showed, that the dynamics and structure are not invariant on the configurational adiabats by using the method described in section 3.5 to step out the configurational adiabat from small changes in density. The reason for this is presumably that the fast vibrations of the intramolecular springs contributes to the configurational entropy used to identify isomorphs.

Despite this, the authors where able to use empirical density scaling to find lines in the (ρ, T)-phase plane, along which the dynamics and structure are invariant in reduced units. Since the lines are not true isomorphs, they have been named *pseudo*isomorphs, due to their isomorph like behaviour. This part of the thesis deals with these and provides ways of identifying the pseudoisomorphic state points with out the need for empirical density scaling.

5.2 Models

This section deal primarily with two molecular models.

The first is a simple asymmetric dumbbell model that was originally introduced in [40] as a toy model of toluene. The model consist of two Lennard-Jones particles, a large and an small one, and was originally modeled with a fixed constraint on the intramolecular distance with length $l_0 = 0.584$ but we use it here with a harmonic

bond potential of the same length and with strength $k_0 = 3000$. The non-bonded potentials are of the Lennard-Jones type

$$v_{ij}(r_{ij}) = 4\epsilon_{ij}\left[\left(\frac{\sigma_{ij}}{r_{ij}}\right)^{12} - \left(\frac{\sigma_{ij}}{r_{ij}}\right)^{6}\right] \tag{5.1}$$

The model parameters are as follows: $\epsilon_{AA} = 1.0$, $\sigma_{AA} = 1.0$ and $m_A = 1.0$, $\epsilon_{BB} = 0.117$, $\sigma_{BB} = 0.788$ and $m_B = 0.195$. For mixing interaction the Lorentz-Berthelot rules are used

$$\epsilon_{AB} = \epsilon_{BA} = \sqrt{\epsilon_{AA}\epsilon_{BB}} \tag{5.2}$$

$$\sigma_{AB} = \sigma_{BA} = \frac{\sigma_{AA} + \sigma_{BB}}{2} \tag{5.3}$$

The figure 5.1 shows the fluctuations in U and W for this model, both when the

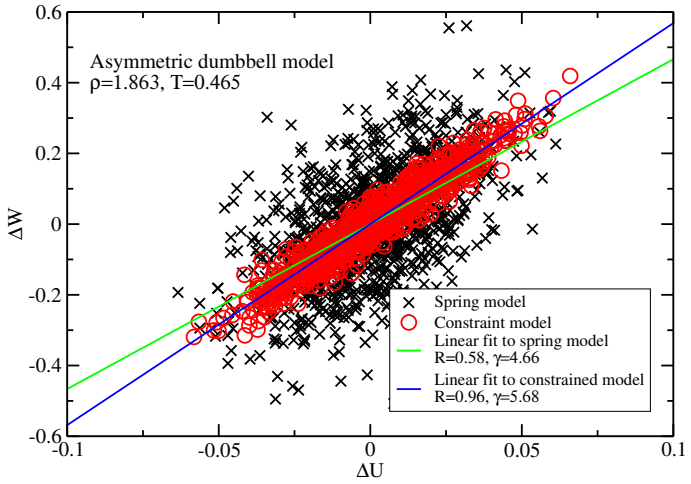

Figure 5.1: The figure shows the fluctuations in potential energy and virial for the asymmetric dumbbell model, comparing two different types of bonded interactions. The black crosses are the model with harmonic springs and the red circles are with a fixed constraint. Both are simulated at $(\rho, T) = (1.863, 0.465)$, a reference state point taken from [29]. It is very clear that the correlation coefficient drops drastically when the harmonic bonds are used. With a correlation of $R_S = 0.58$ we do not expect the system to have isomorphs. Also shown is the scaling parameter $\gamma_S = 4.66$, which also decreases from the one found in the constraint model $\gamma_C = 5.68$.

bonded interactions are harmonic springs and when they are fixed constraints. It was shown in [29], that the model with intramolecular constraints does have isomorphs, which is also indicated by the high correlation coefficient, $R_C = 0.96$. From the spread in the data it is clear that the correlation is worse for the model with harmonic springs, with $R_S = 0.58$, and we do not expect this model to have isomorphs.

The second model used is identical to the one used in [66]. It is a 10 bead linear chain molecular model with bonded interactions given by a harmonic spring potential

with length $l_0 = 1.0$ and strength $k_0 = 3000$. All atoms are of the same type and the non-bonded potential is a Lennard-Jones potential with parameters $\epsilon = 1.0$, $\sigma = 1.0$ and $m = 1.0$. This model have been investigated in great detail both with intramolecular constraint, harmonic bond and FENE potential. For detail we refer to [65,66]. The figure 5.2 shows the fluctuations in U and W for the Lennard-Jones chain

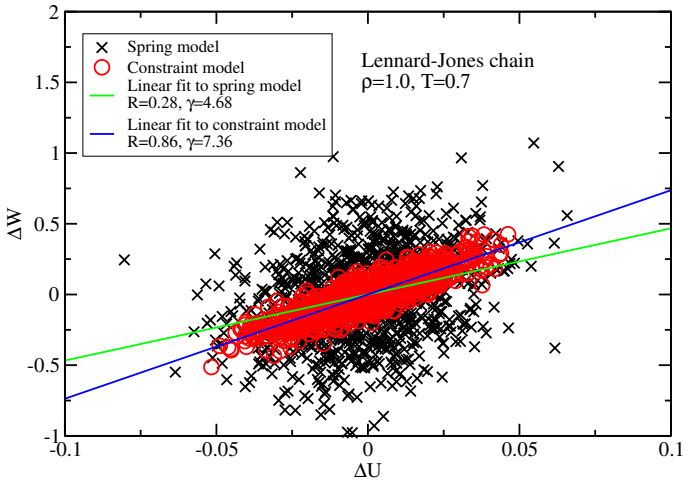

Figure 5.2: Similar to figure 5.1, the figure shows the fluctuations in potential energy and virial but for the Lennard-Jones chain model, with harmonic springs and fixed constraint. The data is from the state point $(\rho, T) = (1.00, 0.70)$, a reference state point taken from [66]. Also here, the correlation coefficient is much lower for the system with harmonic springs with $R_C = 0.86$ and $R_S = 0.28$. Comparing to the asymmetric dumbbell model the correlation coefficient is lower even for the system with constraint. The constraint scaling parameter $\gamma_C = 7.36$ is higher than that of the asymmetric dumbbell model but the spring parameter $\gamma_S = 4.68$ is comparable to that of the asymmetric dumbbell.

model in both the constrained and harmonic spring version. As with the asymmetric dumbbell model, the correlation coefficient is much higher for the constrained model, $R_C = 0.86$ than the spring model $R_S = 0.28$. Despite the correlation coefficient of the constrained model being below $R = 0.9$ it was shown in [65], that this model does have isomorphs.

For both models it is clear that the substitution of the fixed constraints with harmonic springs greatly changes the shape of the configurational adiabat. Interestingly the scaling coefficient $\gamma_S^{LJC} = 4.68$ for the spring model is comparable to that for the asymmetric dumbbell model where $\gamma_S^{ASD} = 4.66$, while for the constraint models the values, $\gamma_C^{ASD} = 5.68$ for the asymmetric dumbbell model and $\gamma_C^{LJC} = 7.36$ for the Lennard-Jones chain model, are quite different. This could be an indication of the effect of harmonic bonds on the excess entropy.

Since both these models have low correlation coefficient with intramolecular springs we do not expect them to have isomorphs.

5.3 Configurational adiabat

In order to test whether the models have isomorphs we trace out the configurational adiabat and measure the dynamics at different state points along it. As mentioned this was done for the Lennard-Jones chain model with harmonic springs in [66], showing that the model does not have isomorphs. We do it here for the asymmetric dumbbell model to illustrate the effect. Taking as a reference state point the state point used in figure 5.1, $(\rho, T) = (1.863, 0.465)$ we get a set of state points along the configurational adiabat. The figure 5.3 shows the intermediate scattering function calculated at

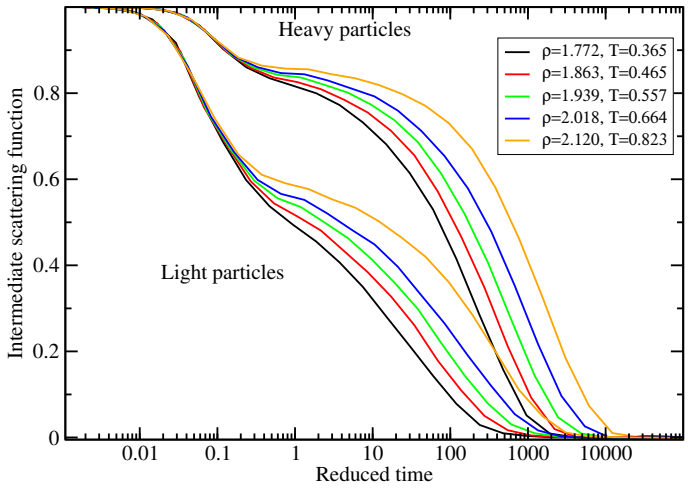

Figure 5.3: The figure shows the intermediate scattering function for the light and heavy particle measured on state points along a configurational adiabat. The data is shown as a function of reduced time and at a constant reduced q, meaning that if the system had isomorphs the data would all collapse to a good approximation. This clearly shows, that the asymmetric dumbbell model with harmonic springs does not have isomorphs.

state points along this configurational adiabat for the light and heavy particles of the asymmetric dumbbell model. The data is presented in reduced units and at constant reduced q-value, corresponding to the main peak in the static structure factor at the reference state point. If the system had isomorphs the data would collapse to two curves, showing that the system does not have isomorphs.

On figure 5.4 we have shown the change in structure along the configurational adiabat, measured as the radial distribution function of the heavy-heavy and light-light pair distances. Here the data almost collapse which, if taken with out the data for the dynamics, could lead to the assumption that the system have isomorph. We attribute this to the fact, that the system is quite dense so structure does not change a lot with state point. Due to this, we will not focus on the structure when identifying pseudoisomorphic state points in the following chapters.

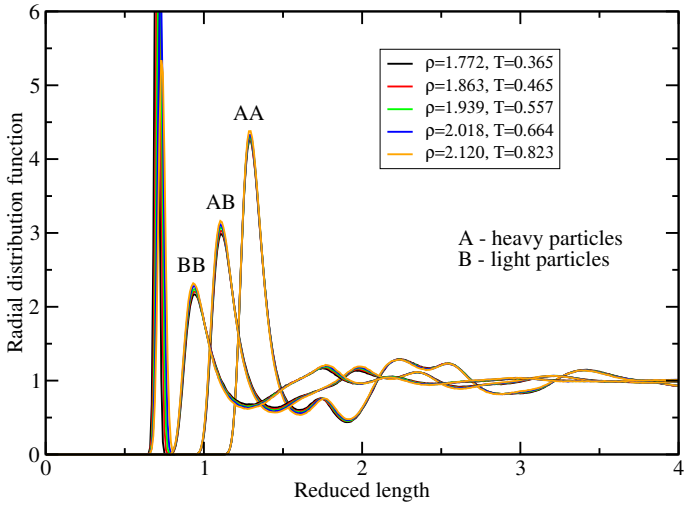

Figure 5.4: The radial distribution function for the light-light and heavy-heavy particle distances measured along a configurational adiabat, in reduced units. Here the data almost collapses. We attribute this to the fact that the system is very dense, so that structure does not change much with state point in general.

5.4 Empirical density scaling

Here we show that it is possible to use empirical density scaling to obtain state points of invariant dynamics for systems with intramolecular springs. These lines was what the authors of [66] called the pseudoisomorphs. The figure 5.5 shows the empirical density scaling of the asymmetric dumbbell model. Three dynamical measures have been calculated along different isochores, resulting in the top panel of the figure. The top panel shows the data plotted as a function of the inverse temperature. The measures used are the relaxation times of the heavy and light particle intermediate scattering function and the center of mass diffusion coefficient. By scaling the heavy particle intermediate scattering function by hand, and applying the same density dependent scaling $h(\tilde{\rho}) = h(\rho/\rho_0)$ to all quantities, the data collapses to a good approximation, see the bottom panel of figure 5.5. This type of scaling resembles that done in experiments to get a scaling coefficient γ.

On figure 5.6 the scaling parameter $h(\tilde{\rho})$ is shown as a function of the reduced density $\tilde{\rho} = \rho/1.863$. The data have been fitted by two different function, a power law function $h_{pl}(\tilde{\rho}) = \tilde{\rho}^{5.43}$, similar to the ones used for empirical density scaling in experiments, and a function similar to the one used to fit the Lennard-Jones chain data in [66], $h(\tilde{\rho}) = 2\tilde{\rho}^{\alpha} - \tilde{\rho}^{\beta}$, with $\alpha = 3.68$ and $\beta = 1.81$. For small density changes these collapse, but for larger, they are clearly different, and even for the $\sim 10\%$ density change shown here it is clear that h_{pl} does not a fit as well. This is not surprising since it has one less free parameter than the other but does underline, that simple power law scaling is only a practical approximation.

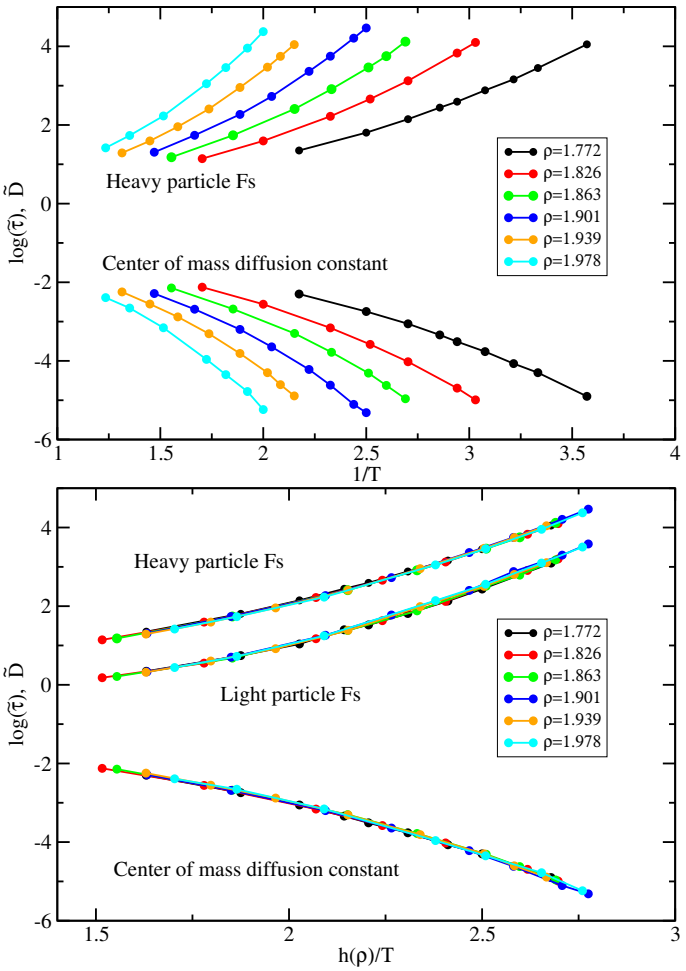

Figure 5.5: Density scaling of different dynamical measures along several isochores for the asymmetric dumbbell model. The figure includes the relaxation times from the intermediate scattering function for the heavy and light particles and the center of mass diffusion constant. The top panel shows the reduced quantities plotted against the inverse temperature. Here the light particle data have been omitted for clarity. In the bottom panel the relaxation time of the heavy particle intermediate scattering function have been scaled by hand to get invariant dynamics giving an empirical $h(\rho/\rho_0)$. The remaining quantities have the been plotted with this scaling $h(\rho/\rho_0)$, to show that all the dynamical quantities collapse to a good approximation with the same scaling factor.

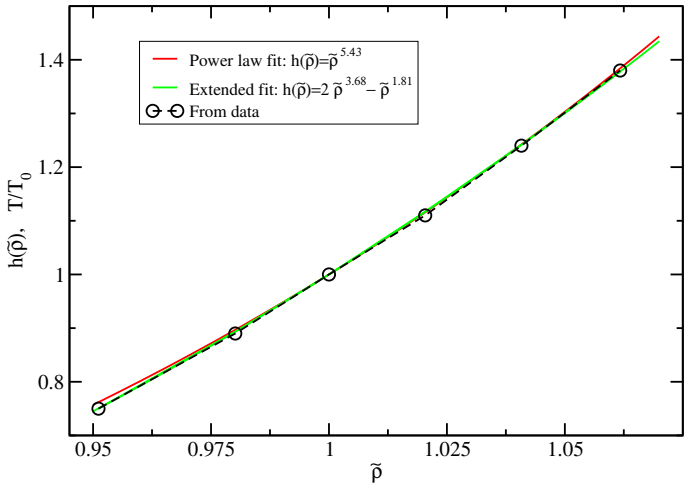

Figure 5.6: The scaling parameter $h(\tilde{\rho})$ as a function of reduced density $\tilde{\rho} = \rho/1.863$ found from the density scaling of figure 5.5. The data have been fitted by both a power law function, giving a function $h_{pl}(\tilde{\rho}) = \tilde{\rho}^{5.43}$ and, similar to what is done for the Lennard-Jones chain in [66], a function $h(\tilde{\rho}) = 2\tilde{\rho}^{3.68} - \tilde{\rho}^{1.81}$. Even over the $\sim 10\%$ density change there are indications that the power law function only works for small density changes.

From the function, it is possible to extract a scaling parameter through

$$\gamma = \frac{d \ln h(\tilde{\rho})}{d \ln \tilde{\rho}} \tag{5.4}$$

For the power law scaling function it is simply $\gamma_{pl} = 5.43$ and for the other

$$\gamma(\tilde{\rho}) = \frac{2\alpha\tilde{\rho}^{\alpha} - \tilde{\rho}^{\beta}}{2\tilde{\rho}^{\alpha} - \tilde{\rho}^{\beta}} \tag{5.5}$$

$$= \frac{7.36\tilde{\rho}^{3.68} - 1.81\tilde{\rho}^{1.81}}{2\tilde{\rho}^{3.68} - \tilde{\rho}^{1.81}} \tag{5.6}$$

which gives $\gamma(1.0) = 5.55$, slightly different from the power law scaling parameter.

This gives us an idea of the shape of the pseudoisomorph and when presenting methods for finding the pseudoisomorphs we will be able to compare the found state points to those given by the density scaling presented here.

6 Scaling of effective springs

In the chapter we develop a method for identifying the pseudoisomorphic state points for the two presented models. We introduce a new isomorph invariant, showing that the reduced eigenvalues of the potential energy Hessian are invariant for isomorphic systems. The method presented here utilizes this new isomorph invariant together with the fact that for the molecular models the eigenvalues separate into those that are related to the model bonds and those that are not. We use this to predict pseudoisomorphic state points.

From the definition of isomorph theory, presented in chapter 3, we know that, if $\mathbf{R}_1$ and $\mathbf{R}_2$ are two physically relevant micro configurations from two different isomorphic state points, that have the same reduced coordinates $\rho_1^{1/3}\mathbf{R}_1 = \rho_2^{1/3}\mathbf{R}_2 = \tilde{\mathbf{R}}$, then the potential energy obeys [52]

$$U(\mathbf{R}_2) \cong f_1(\rho_2, U(\mathbf{R}_2)) \tag{6.1}$$

where f_1 is a state point dependent one-to-one mapping. In a more macroscopic way the means that large parts of the potential energy surface (PES) scales in a simple manner. Inspired by this we test whether the local curvature of the PES is invariant for isomorphic state points.

6.1 The local potential energy surface

We do so by calculating the potential energy Hessian $\mathcal{H}(\mathbf{R})$ at a specific micro configuration. Recall that for a system of N particles the Hessian is a $3N \times 3N$ matrix defined as

$$\mathcal{H}_{i,j}(\mathbf{R}) = \frac{\partial^2 U(\mathbf{R})}{\partial q_i \partial q_j} \tag{6.2}$$

where q is a given component of the $3N$ dimensional position vector $\mathbf{R}$.

Since all potentials used here are pair potentials, the elements of the Hessian fall

in four categories as follows

$$\mathcal{H}_{\alpha_i,\alpha_i} = \sum_{j\neq i} \left[u2(r_{ij})(\alpha_i - \alpha_j)^2 + u'(r_{ij})/r_{ij}\right], \tag{6.3}$$

$$\mathcal{H}_{\alpha_i,\beta_i} = \sum_{j\neq i} u2(r_{ij})(\alpha_i - \alpha_j)(\beta_i - \beta_j), \tag{6.4}$$

$$\mathcal{H}_{\alpha_i,\alpha_j} = -\left(u2(r_{ij})(\alpha_i - \alpha_j)^2 + u'(r_{ij}/r_{ij}\right), \qquad (j \neq i) \tag{6.5}$$

$$\mathcal{H}_{\alpha_i,\beta_j} = u2(r_{ij})(\alpha_i - \alpha_j)(\beta_i - \beta_j), \qquad (j \neq i) \tag{6.6}$$

where i, j denotes the particle, α and β are distinct components of the position of the given particle and

$$u2(r_{ij}) \equiv \left[u''(r_{ij}) - u'(r_{ij})/r_{ij}\right]/r_{ij}^2 \tag{6.7}$$

with u' and u'' being the first and second order derivative of the pair potential with respect to the interparticle distance

$$u'(r_{ij}) = \frac{du}{dr_{ij}}, \quad u''(r_{ij}) = \frac{d^2u}{d(r_{ij})^2} \tag{6.8}$$

The notation is borrowed from [59].

Investigating systems through the energy landscape is hardly a new idea [70].

By calculating the eigenvalues of the Hessian we obtain a set of primary curvatures of the PES. It is customary to express these eigenvalues λ_i as eigenfrequencies ω_i of the system, but we have chosen to express them as effective springs strengths k_i instead, $\lambda_i = 2k_i$, since this makes for a more direct comparison to the strength of the intramolecular bonds of the models used. The eigenvalues were found using the Python package NumPy [62].

The Hessian was calculated in inherent states (IS), i.e. local potential energy minimas. These where found using a simple steepest descend algorithm, where the velocities of the particles where set to zero at each time step. This makes the system move in the direction of the force $\mathbf{F} = -\nabla U$ at all times, eventually leading to the local minima. Though faster and potentially more stable methods exists [13, 43], for the scope of this investigation, this simple algorithm was sufficient.

6.2 A new isomorph invariant

In order to test whether the curvature is an isomorph invariance we calculated the Hessian for the well known Kob-Andersen binary Lennard-Jones mixture [32], known from literature to be an isomorphic system [23].

An equilibrium simulation was performed in the NVT-ensemble for the KABLJ at $(\rho_1, T_1) = (1.228, 0.557)$. From this an equilibrium micro configuration $\mathbf{R}_1$ was picked out and quenched to the local IS, $\mathbf{R}_{1,\mathrm{IS}}$, and the effective springs corresponding to eigenvalues of the Hessian were determined. Simultaneously the equilibrium configuration was scaled to a different density ρ_2, i.e. $\mathbf{R}_2 = (\rho_2/\rho_1)^{-1/3}\mathbf{R}_1$. The scaled micro configurations was quenched at ρ_2 to $\mathbf{R}_{2,\mathrm{IS}}$ and the resulting effective springs compared to those at the reference state point. Such spectra are shown on the top panel of figure 6.1, for density changes in either direction.

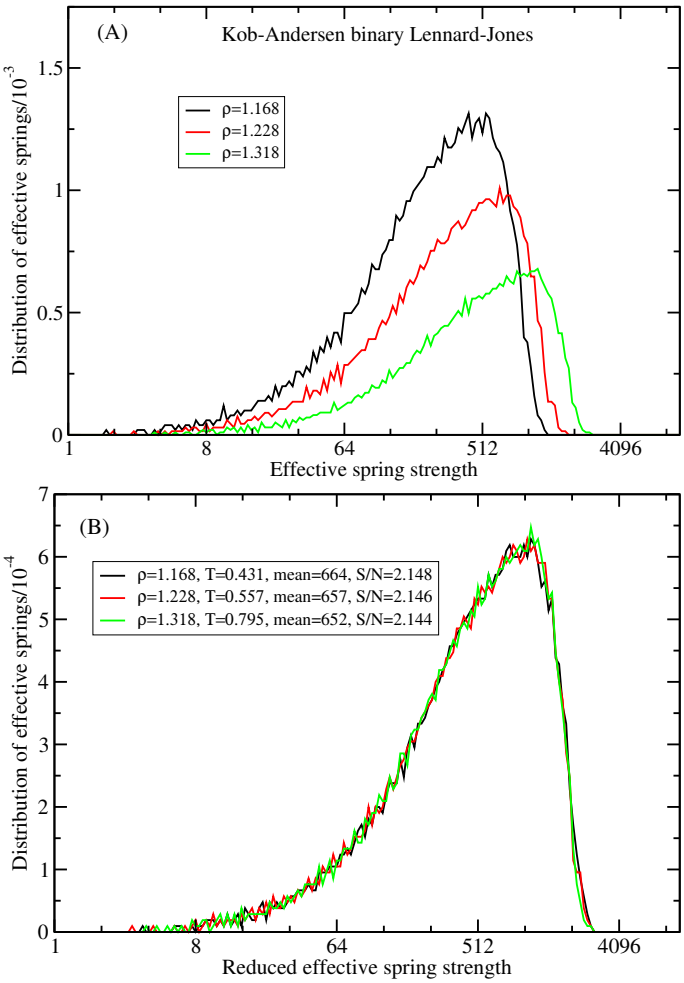

Figure 6.1: The normalized effective spring strength spectrum of the KABLJ mixture. These where calculated at different densities, by scaling an equilibrium micro configuration at $(\rho, T) = (1.228, 0.557)$ to different densities, and then calculating the Hessian at the associated IS at each density. On the top panel (A) the effective spring spectra are presented as calculated and on the bottom panel (B) the same data is shown but for the reduced effective springs. The collapse of the data on the bottom figure shows that the curvature of the PES is an isomorph invariant.

To test for isomorphic invariance, the effective springs k_i were calculated in reduced units $\tilde{k}_i$ as

$$\tilde{k}_i = k_i/(\rho^{2/3} k_B T) \tag{6.9}$$

For the reference effective springs, ρ and T are given by the state point at which the equilibrium simulation is performed. For the scaled effective springs, we use the literature values of the isomorphic state points at the scaled densities,

$$(\rho, T) = (1.168,\, 0.431), \quad (\rho, T) = (1.318,\, 0.795) \tag{6.10}$$

As shown on the bottom panel of figure 6.1, this resulted in approximately invariant spectra showing that the local curvature of the PES is in fact an isomorph invariant.

6.3 The effective spring spectrum of a molecular system

As each eigenvalue corresponds to the curvature in some direction on the PES, we test if the intramolecular springs are visible in the spectrum. A spring should, due to the high spring strength $k = 3000$ result in a large curvature in one particular direction per spring.

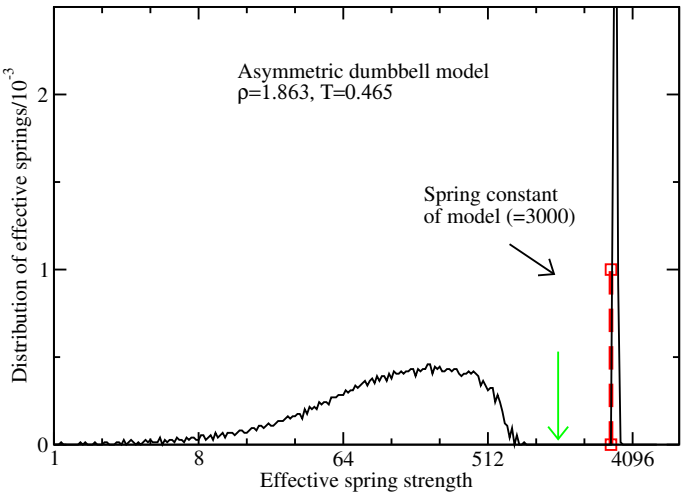

Figure 6.2: The spectrum of effective springs strengths calculated from a single inherent state as the eigenvalues of the Hessian for the asymmetric dumbbell model. Marked with a dashed red line is the spring constant of the model, $k_0 = 3000$. The arrow indicate the separation between the low and high strength springs. The number of effective springs above this separation matches the number of harmonic bonds in the system.

Figure 6.2 shows a spectrum of effective springs calculated for the asymmetric dumbbell model. The spectrum clearly separates into two parts. In the high end of the spectrum is one part where the effective spring strength are comparable to the model spring strength, marked with a red dashed line. These seems to be directly connected

to the springs of the molecular models, both because of the value and because the number of such springs perfectly matches the number of bonded interactions in the system. In the other end are the remaining springs, characterized by a relatively low spring strengths. The two parts are separated by a clear region where there are no effective springs, indicated by the green arrow on the figure.

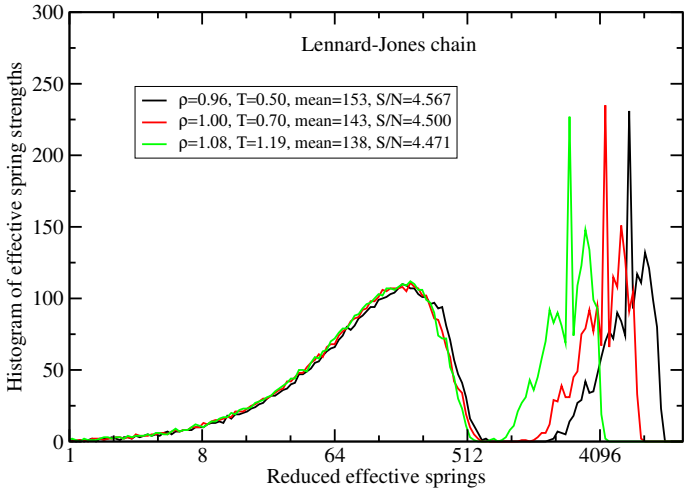

Figure 6.3: Histograms of effective springs calculated for the LJC model at three different densities. The effective springs have been reduced with temperatures from the empirical formula for pseudoisomorphic state points from [66]. While the low end of the histogram seems to collapse to a good approximation, the high end of the spectra does not. This indicates, that scaling eigenvalue spectra can be used to find pseudoisomorphic state points.

Inspired by the scaling behavior of the spectrum for the KABLJ system, we test how the spectrum of the pseudoisomorphic Lennard-Jones system behaves. On figure 6.3 the reduced effective spring spectrum of the Lennard-Jones chain model is shown for three densities. The spectra was created in the same way as the KABLJ spectra, and were reduced by the temperatures given in [66], that resulted in invariant dynamics. The shift in the high end of the histograms seems to come exclusively from the fact that the model spring strength is not the same, when calculated in reduced units. For the low strength part of the figure, the three spectra collapses showing that also pseudoisomorphic state points obey this new isomorph invariant.

Having shown that the effective spring spectrum separates into stronger and weaker springs, corresponding to more and less curved parts of the local PES, and that the weaker effective springs scale in an isomorphic way, we wish to exploit this in order to find pseudoisomorphic state points. The question then becomes how to quantify the collapse of the low end of such a spectrum. In the following sections we present two different approaches to this.

Much like the direct isomorph check, described in section 3.5, we will use our reference state point (ρ_1, T_1), and then pick a different density ρ_2 and attempt to find the temperature T_2 so that the state point (ρ_2, T_2) is pseudoisomorphic to (ρ_1, T_1). In the direct isomorph check, one compares the potential energies of at comparable

micro configurations $\mathbf{R}_1$ and $\mathbf{R}_2$, where $\mathbf{R}_2$ is constructed as

$$\mathbf{R}_2 = \frac{\rho_2}{\rho_1}^{-1/3}\mathbf{R}_1 \tag{6.11}$$

We use a similar $\mathbf{R}_2$, but instead we take this to be the micro configuration at ρ_2 that are quenched to the local IS. The resulting two spring strength spectra should reveal the scaling between the PES at the two densities.

6.4 Proportional springs

Since the spectrum of reduced effective springs is invariant, the individual effective springs should also be invariant to a good approximation. By sorting the effective springs by their strength and comparing two such sorted sets, we hope to compare springs, that correspond to the same curvature of the PES. Using this we get

$$\begin{aligned} \tilde{k}_1^i \approx & \tilde{k}_2^i \\ \frac{k_1^i}{\rho_1^{2/3} k_B T_1} = & \frac{k_2^i}{\rho_2^{2/3} k_B T_2} \\ k_1^i \left(\frac{\rho_2}{\rho_1}\right)^{2/3} \frac{T_2}{T_1} = & k_2^i \end{aligned} \tag{6.12, 6.13}$$

where the i refers to number in the sorted set of effective springs. As the proportionality constant depends on temperature, T_2 can be found from the the relationship between k_1^i and k_2^i.

Such a proportionality can be seen on figure 6.4 for the asymmetric dumbbell model and figure 6.5 for the Lennard-Jones chain. The figures shows the proportionality for the low strength springs for different densities, with respect to the reference densities, for sets of sorted effective springs. The large figures are a zoom in on the low strength part, and the inserts shows the full figure. It is clear in both cases that the high strength springs scale differently from the low strength ones. The full lines are the symmetric slope of the data, and the dashes is a line of slope 1.0.

In both cases the low strength springs are proportional to a good approximation.

In order to get T_2 we look at the variance of the low strength spring constants $\langle(\Delta k)^2\rangle$ corresponding to the symmetric slope of the data in figures 6.4 and 6.5. Defining

$$\alpha \equiv \frac{\langle(\Delta k_2)^2\rangle}{\langle(\Delta k_1)^2\rangle} \tag{6.14}$$

which we can access from the data, we can compare the variance of the reduced spring strengths to get an estimate of T_2,

$$\begin{aligned} \langle(\Delta \tilde{k}_1)^2\rangle = & \langle(\Delta \tilde{k}_2)^2\rangle \\ \frac{\langle(\Delta k_1)^2\rangle}{(\rho_1^{2/3} T_1)^2} = & \frac{\langle(\Delta k_2)^2\rangle}{(\rho_2^{2/3} T_2)^2} \\ T_2 = & T_1 \sqrt{\alpha} \left(\frac{\rho_1}{\rho_2}\right)^{2/3} \end{aligned} \tag{6.15}$$

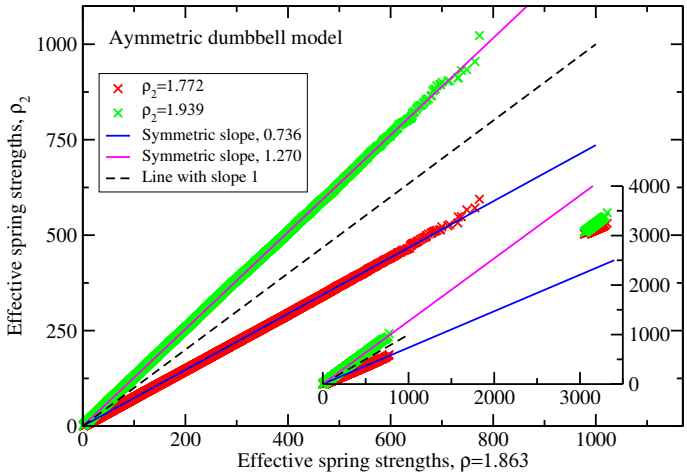

Figure 6.4: The sorted effective spring strengths at the reference state point, plotted against the effective spring strengths at state points with densities slightly below and above the reference density, for the asymmetric dumbbell model. The approximate proportionality between the low spring strength eigenvalues is quite clear. For both density changes, the correlation coefficient is 0.999. The primary figure is a zoom in on only the low strength effective springs where as the insert is the complete spectrum showing clearly the separation between weak and strong springs, as well as the fact that the high strength springs does not scale in the same way as the low strength ones.

Though it is in principle possible to get an estimate of the temperature T_2 from a single comparison of spectra, it makes sense to use a series of comparisons to increase the accuracy. The effect of this is shown on figure 6.6 for the asymmetric dumbbell model, where the estimated T_2 is plotted as a function of the number of spring strength comparisons made normalized with the temperature estimated after 4096 comparisons. It shows that even very few comparisons give a good results deviating by less than a percent. For the Lennard-Jones chain model the deviations are larger but still small enough that only a few spectra are needed. In both cases the standard deviation goes as $1/\sqrt{n}$ as expected.

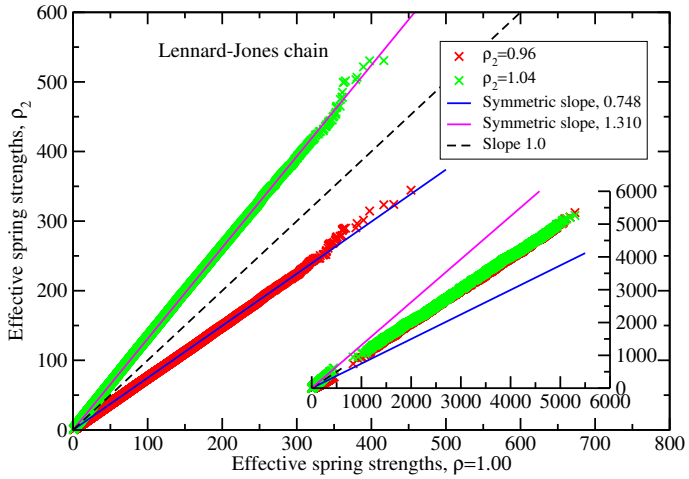

Figure 6.5: Corresponding to figure 6.4, but for the Lennard-Jones chain model. Also here the proportionality between the low strength eigenvalues is quite clear for both an increase and decrease in density, with correlation coefficients close to 1. The separation between weak and strong springs is visible on the insert. Here it is also clear that the scaling is different for the strong and weak springs.

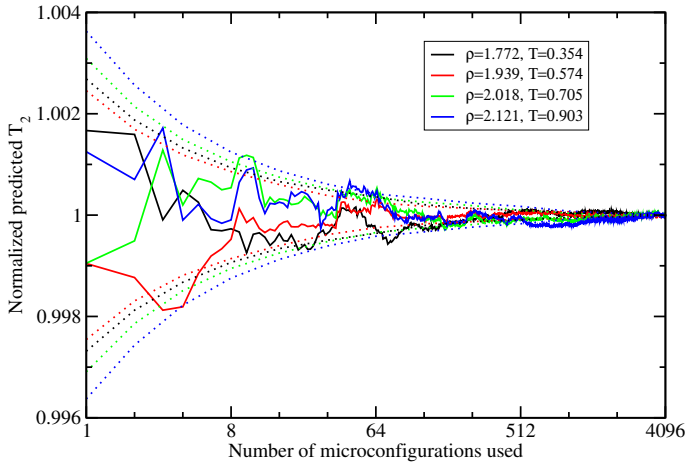

Figure 6.6: The deviation from the predicted T_2 for a set of different density jumps, as a function of micro configurations used to predict the temperature. Also shown is the standard deviation which goes as $n^{-1/2}$ like one would expect.

6.5 The sum of the springs

A different approach is to consider the spectrum rather than the individual springs. Often when people work with the thermodynamics of IS, they use a harmonic approximation of the local curvature [48, 49, 54]. In that case, the quantity L defined as

$$L \equiv \frac{1}{3N-3} \sum_{i}^{3N-3} \log \tilde{k}_i \tag{6.16}$$

where $\tilde{k}_i$ is the reduced k_i, is used to estimate the free energy [48] or entropy [54] associated to the basin surrounding an IS. Note that the sum exclude the 3 eigenvalues that are zero due to the periodic boundary conditions. This L can be related to the non-reduced springs as

$$S = \sum_{i}^{3N-3} \log(k_i/\rho^{2/3} k_B T) \tag{6.17}$$

$$= \sum_{i}^{3N-3} \log(k_i) - (3N-3)\log(\rho^{2/3} k_B T) \tag{6.18}$$

Calculating L for the KABLJ system from the three spectra shown in figure 6.1, gives the values

$$\rho = 1.168, \quad L/(3N-3) = 2.148 \tag{6.19}$$

$$\rho = 1.228, \quad L/(3N-3) = 2.146 \tag{6.20}$$

$$\rho = 1.318, \quad L/(3N-3) = 2.144 \tag{6.21}$$

values that are very close to constant. In order to apply the same measure to the molecular models, we define the similar quantity L_{PI} for the systems with springs,

$$L_{PI,1} = \sum_{i}^{3N-(n_S+3)} \log(k_i^{(1)}) - (3N-(n_S+3))\log(\rho_1^{2/3} k_B T_1) \tag{6.22}$$

where n_S are the number of harmonic bonds in the system. Calculating this for the histograms of the Lennard-Jones chain model, using the short hand notation $N_{PI} = 3N - (n_S + 3)$, gives

$$\rho = 0.96, \quad L_{PI}/N_{PI} = 4.567 \tag{6.23}$$

$$\rho = 1.00, \quad L_{PI}/N_{PI} = 4.500 \tag{6.24}$$

$$\rho = 1.08, \quad L_{PI}/N_{PI} = 4.471 \tag{6.25}$$

The deviation in these numbers are slightly larger than those of the KABLJ system, but as the isomorph theory is approximate in nature, we expect some variation. In both cases the deviations seems to be a systematic, with higher density leading to lower L or L_{PI} values.

To use this formulation to predict the pseudoisomorphic state points we use that for pseudoisomorphic state points, the L_{PI} values should be constant. Defining

$$s_1 = \sum_{n}^{N_{PI}} \log(k_n^{(1)}) \tag{6.26}$$

we can see that the temperature T_2 that gives invariant L_{PI}-values can be found as

$$\begin{aligned} L_{PI,1} &= L_{PI,2} \\ s_1 - N_{PI}\log(\rho_1^{2/3}k_BT_1) &= s_2 - N_{PI}\log(\rho_2^{2/3}k_BT_2) \end{aligned} \tag{6.27}$$

giving

$$T_2 = T_1\left(\frac{\rho_2}{\rho_1}\right)^{2/3}\exp\left[\frac{s_2 - s_1}{3N - (n_S + 3)}\right] \tag{6.28}$$

As above we calculate the right hand side of the equation for a large number of IS, using the average T_2 as the pseudoisomorphic temperature.

6.6 Applying the two methods

The above section gives two methods of identifying pseudoisomorphs based on the effective springs calculated from the potential energy Hessian.

The first method defined by equation (6.15), where T_2 is estimated from the proportionality of the sorted effective springs at different densities, and the second, defined by equation (6.28), where T_2 is estimated from the invariance in the value $L_{PI} = \sum_n^{N_{PI}} \log \tilde{k}_n$.

The temperatures found by the two methods are shown in figure 6.7. The top panel shows the temperatures found for the asymmetric dumbbell model, and the bottom panel for the Lennard-Jones chain model. Both figures also include the empirical estimate of the temperature found from density scaling, taken from section 5.4 for the asymmetric dumbbell model and from [66] for the Lennard-Jones chain. None of the models gives a perfect match to the empirical estimate of the temperature, but it seems that the method using the L_{PI}-value gives the best fit.

From simulations at the state points generated from the proportionality of the sorted springs, we are able to compare the reduced dynamics, to test if they are in fact invariant. The figures 6.8 and 6.9 show the dynamic measured as the intermediate scattering function for the asymmetric dumbbell model and the Lennard-Jones chain model respectively.

In figure 6.8 the intermediate scattering function is shown for the light and heavy particles separately, at constant reduced q-value, corresponding to the first peak of the structure factor at the reference state point. The collapse is very good, though slightly better for the heavy particles. This might be because the dynamics are dominated by the behaviour of the heavy particles. Similar behaviour is seen for systems with regular isomorphs, For the KABLJ system, which also have heavy and light particles, it has been shown that the structure of the heavy particles collapses better along the isomorph than that of the light particles [23].

Figure 6.9 shows the segmental and center-of-mass intermediate scattering function at constant reduced q-values. Here the collapse is not quite as good as that of the asymmetric dumbbell model. In particular, the low density state point $(\rho, T) = (0.96, 0.546)$ seems to deviate from the rest both in case of the segmental and center-of-mass part. Still, the collapse is far better for the state points found with this method than for the configurational adiabat.

Repeating this procedure for the method with invariant L_{PI}-value results in the data presented in figures 6.10 and 6.11. As was perhaps expected from the predicted temperatures, it seems that the collapse in the latter figures are better than the

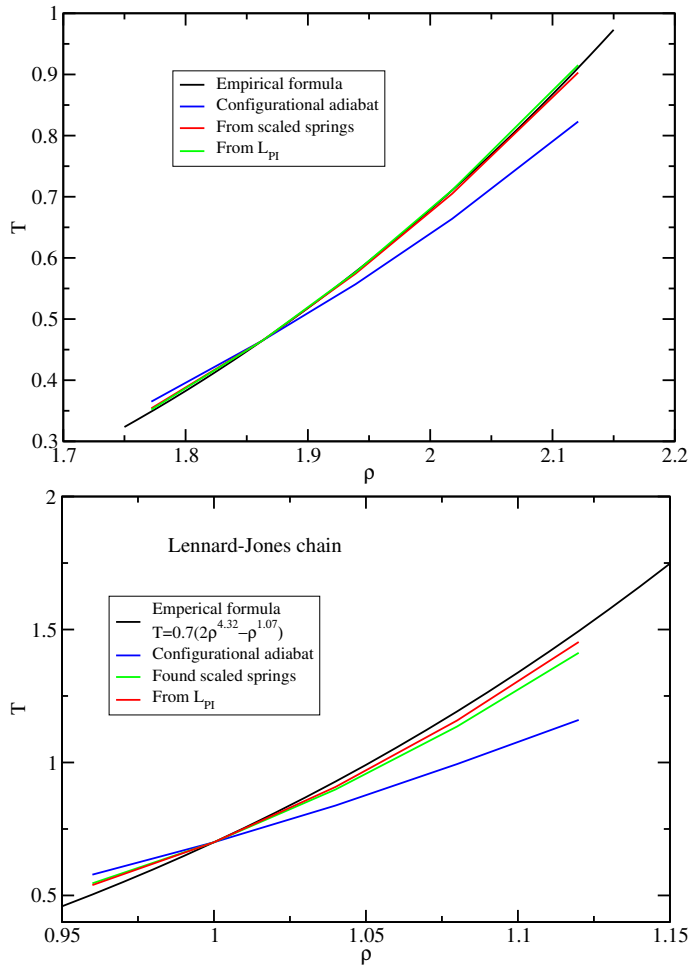

Figure 6.7: The temperature T_2 estimated with the two method described in sections 6.4 and 6.5, for the asymmetric dumbbell model, top panel, and the Lennard-Jones chain model, bottom panel. On both figures the formula derived from empirical density scaling, for the respective model, is included. For neither method the collapse is perfect. The two methods deviate slightly and it seem the method that relies on the value L_{PI} is slightly closer to the empirical estimates.

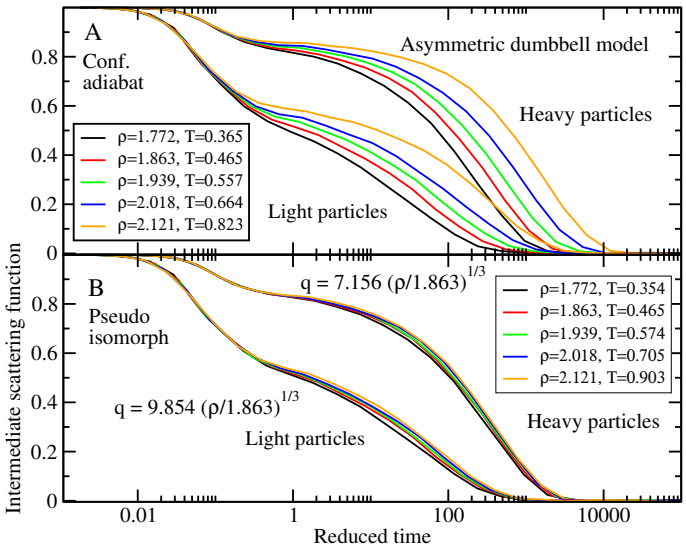

Figure 6.8: The intermediate scattering function of the separate particle types for the asymmetric dumbbell model, plotted as a function of reduced time, for constant reduced q-values. The top panel, (A), shows the intermediate scattering function for state points along the configurational adiabat, mapped out from the reference state points. It is clear that the there is no collapse showing that the asymmetric dumbbell model does not have isomorphs. The bottom panel, (B), shows the same data for state points along the pseudoisomorph mapped out using the method defined in equation (6.15), using the proportionality of the sorted effective springs. The collapse, though not perfect, is remarkable given that the state points used are all predicted using equilibrium micro configurations at a single reference density.

corresponding collapses of figures 6.8 and 6.9, indicating that using the invariance of the L-values give a better estimate of the pseudoisomorphs.

To test how well the last method estimates the invariance of the dynamics we have calculated the reduced relaxation time $\tilde{\tau}$, for three different quantities for the Lennard-Jones chain model, at the state points found with this method. The figure 6.12 shows $\tilde{\tau}$ for the segmental and center of mass intermediate scattering function and for the end-to-end autocorrelation. Also included on the figure is data from an isotherm, the configurational adiabat and the state points found from the empirical formula provided in [66]. Of the four sets of state points it is clear that the pseudoisomorph found here, and the state points found from empirical density scaling gives the most invariant dynamics. By numerically evaluating the derivative

$$\alpha = \frac{d \log \tilde{\tau}}{d\rho} \tag{6.29}$$

it is possible to determine that the pseudoisomorph deviates slightly more from invariance.

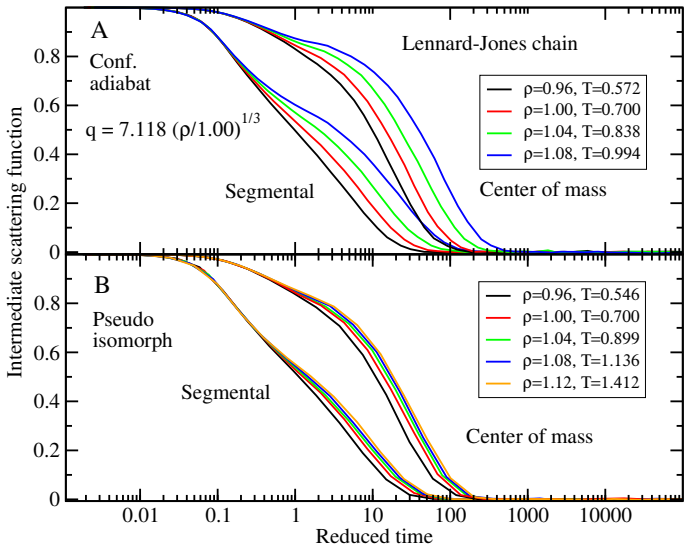

Figure 6.9: The segmental and center of mass intermediate scattering function for the Lennard-Jones chain, plotted as a function of reduced time for a constant reduced q-value. The top panel, (**A**), shows the data for the configurational adiabat starting at the reference state point. The bottom panel, (**B**), shows the data for the pseudoisomorph found by the method presented in this paper. Again the collapse of the pseudoisomorph is quite a lot better than the corresponding configurational adiabat though not nearly as good as the collapse of data presented in [66], where the authors used empirical density scaling.

To test the limit of these methods, we applied it to the asymmetric dumbbell model, but with the spring strength reduced to $k = 250$. On figure 6.13 both the comparison of sorted springs and the distribution of effective spring values is shown. In both cases, it is not clear how to separate out the effective springs related to the model springs. In this case we would not be able to apply these methods.

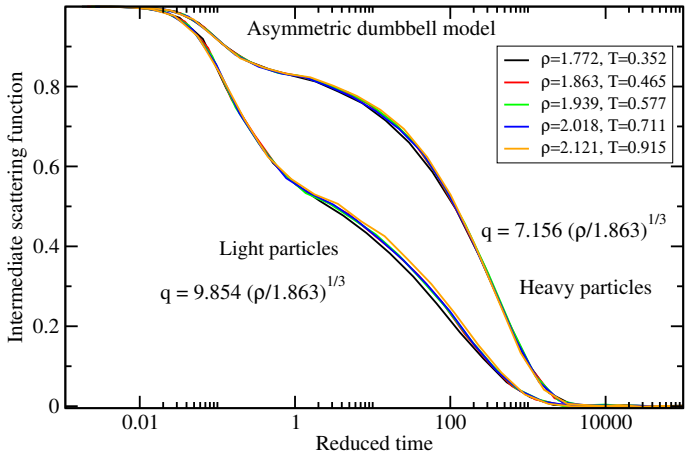

Figure 6.10: The intermediate scattering function of the separate particle types for the ASD model, plotted as a function of reduced time, for constant reduced q-values, for state points found from invariant L_{PI}-values. Compared to the collapse presented in figure 6.8 the collapse is almost perfect for this method.

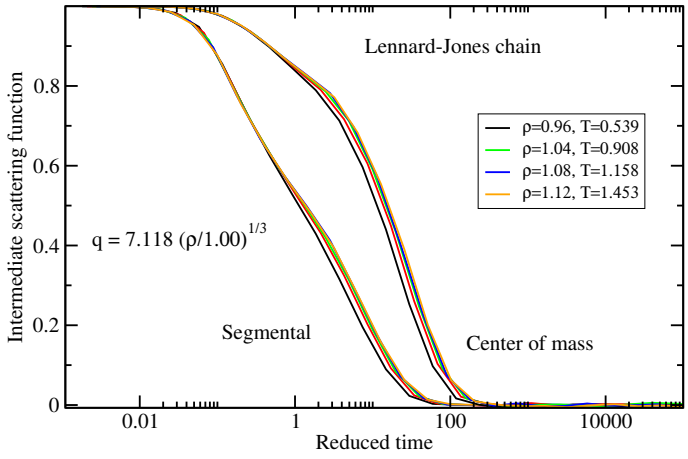

Figure 6.11: The segmental and center of mass intermediate scattering function for the LJC, plotted as a function of reduced time for a constant reduced q-value for state points found from invariant L-values. Again the collapse of the pseudoisomorph is quite a lot better than the corresponding configurational adiabat though not as good as the collapse of data presented in [66], where the authors used empirical density scaling.

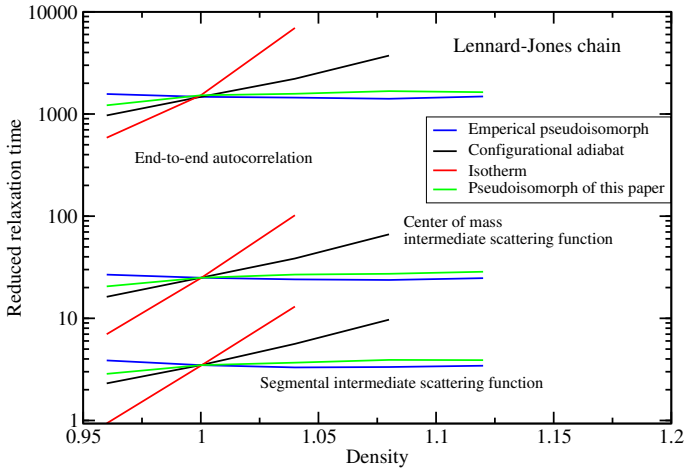

Figure 6.12: Three reduced relaxation times of the LJC model plotted as a function of density along the empirical pseudoisomorph of paper [66], the configurational adiabat, an isotherm and the pseudoisomorph presented in this paper. The relaxation times are from the end-to-end auto correlation, the center of mass intermediate scattering function and from the segmental scattering function. In all three cases it is clear that the pseudoisomorph found in this paper gives almost as good invariance as the state points found with empirical density scaling.

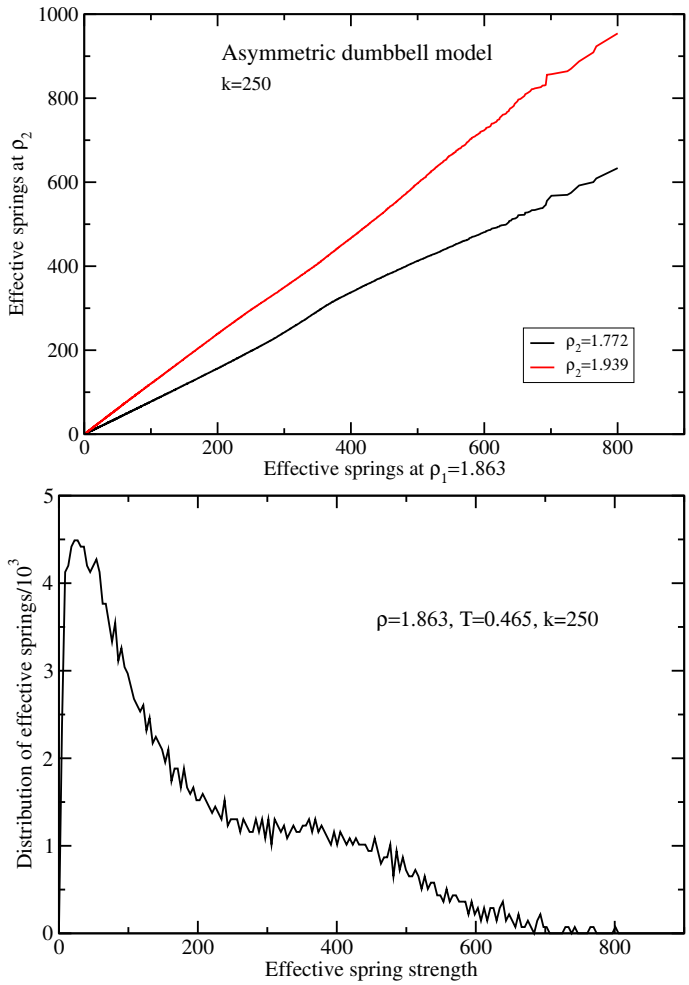

Figure 6.13: The asymmetric dumbbell model with a spring strength of $k = 250$. Here the effective springs related to the model springs does not separate out, neither for the sorted springs, top panel, nor for the distribution, bottom panel. This illustrates the limits of the methods presented here.

6.7 Discussion and conclusion

We have shown for the first time that it is possible to find pseudoisomorphic state points for the two models used here, from the invariance of the curvature of the PES. Specially the method, where the effective spring spectrum was characterized by the L_{PI}-value, resulted in a very good collapse of the dynamics expressed through the intermediate scattering function for both models.

For the Lennard-Jones chain, there where some deviations at low densities when comparing to the invariance along the state points found with empirical density scaling. It is possible that this is due to the low pressure, $P \sim 0.5$ at the state points with this density. The isomorph theory generally breaks down at low pressure [23] which would mean that the isomorphic invariance of the effective spring spectrum does not hold, something that might not be a problem for the empirical density scaling.

As such the method presented here, is not meant to compete with the empirical density scaling, where a large number of simulations or experiments are performed in order to estimate the scaling parameter. The methods presented here gives the scaling parameter from configurations picked out of an equilibrium simulation only at the reference state point. Finding the pseudoisomorphs does however seem to require more work than finding ordinary isomorphs, as the scaled configurations needs to be quenched in order to find the relevant spectra.

7 Free energy scaling

In this chapter we present a different approach to identifying pseudoisomorphic state points. The idea is to generalizes the invariance of Boltzmann probabilities between pseudoisomorphic state points, to an invariance of probabilities in a coarse grained configurational space. This results in 2 different ways of finding pseudoisomorphs, one for each model type. The general method relies on a free energy expression, defined for a configurational space, where the intramolecular vibrations have been integrated out. Also this method makes it possible to identify pseudoisomorphic state points.

7.1 Introduction

In the previous chapter pseudoisomorphs were identified with success from the invariance of parts of the eigenvalue spectra, calculated at different inherent states (IS). The primary tool was the scaling properties of the potential energy surface (PES) between isomorphic state points. This was used together with the fact, that the eigenvalue value spectrum separated into a part related to the model spring and a part related to the remaining degrees of freedom.

In this chapter we present a different approach to finding pseudoisomorphic state points. The reason for introducing another method is that, the method presented in the previous chapter utilizes a particular feature of the two model systems. As was shown on the figure 6.13 it is not always possible to to separate the eigenvalues spectrum into an "isomorphic" and "non-isomorphic" part. We wish to develop a general method that could in principle be applied to any kind of system with pseudoisomorphs. In testing implementations of this method we will be using the same model systems, so the harmonic bonds will still be present.

As was show in chapter 3, for ordinary isomorphic state points (ρ_1, T_1) and (ρ_2, T_2), we have that the probability distribution of a given reduced micro configuration, $\tilde{\mathbf{R}}$, is independent of state point [23,52]. The above criteria can be written as

$$P_1(\tilde{\mathbf{R}}) = P_2(\tilde{\mathbf{R}}) \tag{7.1}$$

$$\exp[-U(\rho_1^{-\frac{1}{3}}\tilde{\mathbf{R}})/k_B T_1] \propto \exp[-U(\rho_2^{-\frac{1}{3}}\tilde{\mathbf{R}})/k_B T_2] \tag{7.2}$$

where the proportionality is due to the normalization, independent of the specific micro configuration. This can not be true for systems with pseudoisomorphs since this would imply isomorphic behavior.

The overall idea of the procedure presented here is to separate the degrees of freedom (DOF) into "isomorphic" I and "non-isomorphic" nI DOF and define a probability function in a reduced space, where the nI DOF have been integrated out. The idea of "isomorphic" and "non-isomorphic" DOF is somewhat abstract, but if one takes as an example the Lennard-Jones chain model, the results from [66] shows that the long time dynamics behave as if the system had isomorphs. Here we advocate that one can think of this as if some of the DOF behave isomorph-like and some do not. This sets a natural limit to the method, since it will only work if the DOF can be separated into two such sets. For the models used here this seems to be the case, since the introduction of harmonic bonds in the models is what caused them to "lose" their isomorphs.

7.2 Proportional reduced space Boltzmann factors

By separating the degrees of freedom into isomorphic and non-isomorphic DOF, R_I and R_{nI}, we can write the probability of a given micro configuration as

$$P(\mathbf{R}) = P(R_I, R_{nI}) = \frac{1}{Z}\exp[-U(R_I, R_{nI})/k_BT] \tag{7.3}$$

Note that R_I and R_{nI} does not in general represent a well know set of Cartesian coordinates only DOF.

In order to integrate out the non-isomorphic DOF we define an isomorphic configurational free energy F^I as a function of a specific value of the the isomorphic DOF,

$$\exp[-F^I(R_I)/k_BT] \equiv \int \mathrm{d}\, R_{nI} \exp[-U(R_I, R_{nI})/k_BT] \tag{7.4}$$

This lets us calculate the probability of a specific value of our isomorphic DOF in the configurational space where the non-isomorphic DOF have been integrated out.

$$P^I(R_I) = \int dR_{nI} P(R_I, R_{nI}) = \frac{1}{Z}\exp[-F^I(R_I)/k_BT] \tag{7.5}$$

where the first equality follows from the statistical independence of all DOF at equilibrium.

In order to compare probabilities at different state points we introduce the abstract notion of reduced degrees of freedom denotes as the other reduced quantities, e.g. $\tilde{R}_I$. To relate, for instance, the probability of a specific value of a reduced DOF to that of the corresponding DOF at (ρ_1, T_1) we will use the subscript 1, i.e. $P_1^I(\tilde{R}_I) \equiv P^I(R_{I,1})$.

Having defined the probability distribution in isomorphic space, we can see that in order for two micro configurations to have the same probabilities for a given value of the reduced isomorphic DOF we have

$$P_1^I(\tilde{R}_I) = P_2^I(\tilde{R}_I) \tag{7.6}$$

$$\exp[-F_1^I(\tilde{R}_I)/k_BT_1] \propto \exp[-F_2^I(R_I)/k_BT_2] \tag{7.7}$$

which gives the defining relation for state points with the same value for the reduced isomorphic DOF

$$-F_1^I(\tilde{R}_I)/k_BT_1 + C = -F_2^I(\tilde{R}_I)/k_BT_2 \tag{7.8}$$

where C is constant for a given set of state points. This equation highly resembles the original formulation of the isomorph theory [23] except that it is free energies rather than potential energies that are compared.

From this it follows that two pseudoisomorphic state points have the same isomorphic free energy for each micro configuration in reduced space, except for an additive constant for a given value of $\tilde{R}_I$. Put in terms of the direct isomorph check, see chapter 3, given a state point (ρ_1, T_1) and a different density ρ_2 we can find the pseudoisomorphic state point by finding the value of T_2 that gives the best approximation to the linear relation in the above expression, when calculating F_1^I and F_2^I for a set of $\tilde{R}_I$'s.

The challenge of this general method is to access the free energy, since this is related to the accessible volume of an entire multidimensional space, meaning that a brute force approach will be impossible. Calculating free energies has almost become an independent branch in condense matter simulations, in particular in biophysics [31]. Different ways of doing this have been suggested in the literature ranging from standard thermodynamic integration to transition path sampling [10], and for any specific type of model system, it may be that a specific solution is needed. Here we present two ways of doing this. The first resembles the method presented by Bennett [8] and relies on the fact that for a simple model, like the asymmetric dumbbell model, it is easy to associate the isomorphic and non-isomorphic DOF to a specific set of Cartesian coordinates, making it possible to simulate in a non-isomorphic space through Monte Carlo simulations. The second uses the fact that the models used here have intramolecular harmonic springs, which makes it possible to approximate the free energy through a harmonic approximation.

7.3 Free energy differences

Rather than trying to calculate the free energies at a given state point, we recast equation (7.8) into

$$-F_2^I(\tilde{R}_I)/k_BT_2 + F_1^I(\tilde{R}_I)/k_BT_1 = C \tag{7.9}$$

The aim is then to shown, that the difference in free energy for configurations with the same value for the reduced isomorphic degrees of freedom is constant.

Imagine we have a state point 1 and want to test whether another state point 2 is pseudoisomorphic to the first. Using the notation $U_1 = U(R_{I,1}, R_{nI,1}) = U(\mathbf{R}_1)$ we can write the exponent to the difference in free energy as

$$\frac{\exp[-F_2^I/k_BT_2]}{\exp[-F_1^I/k_BT_1]} = \frac{\int \mathrm{d}\, R_{nI} \exp[-U_2/k_BT_2]}{\int \mathrm{d}\, R_{nI} \exp[-U_1/k_BT_1]} \tag{7.10}$$

By multiplying the numerator with the constant function $\exp[(-U_1+U_1)/k_BT_1]=1$ and rearranging the exponents, one gets

$$\begin{aligned}\frac{\exp[-F_2^I/k_BT_2]}{\exp[-F_1^I/k_BT_1]} &= \frac{\int \mathrm{d}\, R_{nI} \exp[-U_2/k_BT_2]\exp[(-U_1+U_1)/k_BT_1]}{\int \mathrm{d}\, R_{nI}\exp[-U_1/k_BT_1]} \\ &= \frac{\int \mathrm{d}\, R_{nI} \exp[-U_2/k_BT_2+U_1/k_BT_1]\exp[-U_1/k_BT_1]}{\int \mathrm{d}\, R_{nI}\exp[-U_1/k_BT_1]} \\ &= \langle \exp[-U_2/k_BT_2+U_1/k_BT_1]\rangle_{1,nI}\end{aligned} \tag{7.11}$$

where the subscript $1, nI$ in the final term indicates that the average should be carried out over non-isomorphic micro configurations generated at state point (ρ_1, T_1).

From this we get the difference in free energy as

$$F_2^I/k_BT_2 - F_1^I/k_BT_1 = \ln\left(\langle \exp[-U_2/k_BT_2+U_1/k_BT_1]\rangle_{1,nI}\right) \tag{7.12}$$

which should be approximately constant for any value of the reduced isomorphic DOF. Again it it worth noting, that this way of calculating free energy differences is not related to isomorphs or pseudoisomorphs. The method was originally formulated to calculate the difference in free energy between two known state points [8]. The problem of finding pseudoisomorphic state points is different in that regard, since T_2 is unknown.

As with the direct isomorph check we wish to find the temperature T_2, given the reference state point (ρ_1, T_1) and the density ρ_2. Using equation (7.11) with out knowing T_2 can be done by taking $\mathbf{R}_2$ as for the direct isomorph check

$$\mathbf{R}_2 = \rho_2^{-1/3}\rho_1^{1/3}\mathbf{R}_1 \tag{7.13}$$

and consequently the potential energy

$$U_2 = U(\rho_2^{-1/3}\rho_1^{1/3}\mathbf{R}_1) \tag{7.14}$$

as the potential energy of the micro configuration $\mathbf{R}_1$ scaled to density ρ_2.

From equation (7.12) we have that the difference between isomorphic free energies at two pseudoisomorphic state points must be approximately constant. Being approximately constant is not a very functional property when the constant is unknown, so instead we calculate the difference, $X(T_2) = F_2^I/k_BT_2 - F_1^I/k_BT_1$, and the variance of this difference $\langle(\Delta X)^2\rangle$. For a perfect pseudoisomorphic system, this would be zero exactly since according to equation (7.8) the difference is equal to a constant that only depend on the state point, not the micro configuration.

By calculating this for a given state point (ρ_1, T_1) and a different density ρ_2 and for several different values of T_2 we can get an approximation to the deviation from zero as a function of T_2, and by fitting this to a second order polynomial, we get an approximate expression for the variance, with a minimum that gives the temperature T_2 that should result in pseudoisomorphic behaviour for the chosen density ρ_2.

In the following we apply this method to the asymmetric dumbbell model. There the non-isomorphic DOF are the intramolecular vibrations of which there are one per molecule.

7.4 Simulations in reduced space

The asymmetric dumbbell is a perfect candidate for this procedure, since it is very easy to rewrite the ordinary $3 \times N$ dimensional position vector $\mathbf{R}$ in a form that separates the intramolecular vibrational degrees of freedom from the rest.

For a given molecule n we have two particles A and B. We can write the position of these as

$$\mathbf{r}_{A_n}(t) = \mathbf{r}_{n_{CM}}(t) + \mathbf{A}_n(t), \quad \mathbf{r}_{B_n}(t) = \mathbf{r}_{n_{CM}}(t) + \mathbf{B}_n(t) \tag{7.15}$$

with

$$\mathbf{A}_n(t) = \frac{s_n(t)}{m_A}\hat{\mathbf{r}}_n(t), \quad \mathbf{B}_n(t) = -\frac{s_n(t)}{m_B}\hat{\mathbf{r}}_n(t) \tag{7.16}$$

where $\mathbf{r}_{n_{CM}}$ is the center of mass position of molecule n, s_n is the mass-reduced distance from the center of mass of the molecule to the particles, $m_{A,B}$ is the mass of particles of type A and B respectively and $\hat{\mathbf{r}}_n$ is the orientation of the molecule, given as the unit vector from particle B to particle A. In particular s_n is related to the intramolecular distance as

$$\begin{aligned} |\mathbf{r}_{A,n} - \mathbf{r}_{B,n}| =& \sqrt{\mathbf{A}_n - \mathbf{B}_n} \\ =& \sqrt{\left(\frac{1}{m_A} + \frac{1}{m_B}\right)^2 s_n^2 \hat{\mathbf{r}}_n(t)\hat{\mathbf{r}}_n(t)\hat{\mathbf{r}}_n(t)\hat{\mathbf{r}}_n^2} \\ =& \left(\frac{1}{m_A} + \frac{1}{m_B}\right) s_n \end{aligned} \tag{7.17}$$

Written like this, it is clear that $\mathbf{r}_{n_{CM}}(t)$ and $\hat{\mathbf{r}}_n(t)$ are related directly to the non-vibrational DOF of the molecule and $s_n(t)$ directly to the vibrational one. By fixing $\mathbf{r}_{n_{CM}}(t) = \mathbf{r}_{n_{CM}}(t_0)$ and $\hat{\mathbf{r}}_n(t) = \hat{\mathbf{r}}_n(t_0)$ we are keeping a constant value of the isomorphic DOF, R_I.

From a computational point of view, this could be done in different ways and though we have chosen to use Monte Carlo simulations, it might be that the best solution for a different system is one of the following.

If one wanted to perform molecular simulations in $3 \times N$-dimensions, one could attempt to solve the problem, by applying a constraint potential on the molecular centers of mass and orientations through Gauss principle of least constraints, which states that the acceleration of a system under constraints applied to a system should be so that it minimizes the difference

$$D = \sum_i^N \frac{1}{2m_i}(m_i\ddot{\mathbf{x}}_i - \mathbf{f}_i)^2 \tag{7.18}$$

where $\mathbf{f}_i$ is the unconstrained force acting on the system [21]. In essence, the constrained dynamics be as close as possible to the unconstrained one. Using this formulation, one can correctly define an constraint force. The method has been used with success to constraint the distance between bonded particles [19, 60]. The problem at hand does however require constraints on the rotation of the molecules meaning that the problem becomes very complicated requiring the inclusion of quaternions [2].

Alternatively one could try to formulate the problem as dynamics in $N/2$-dimensions, where each dimension correspond to a $s_n(t)$. This could be done trough a Lagrangian

formulation of the dynamics, see for instance [33]. In this formulation of dynamics, the system is described through generalized coordinates, in case of the asymmetric dumbbell the intramolecular bond lengths s_n. For a Lagrangian $\mathcal{L}(t, S, \dot{S})$ where S is the $N/2$ bond lengths and $\dot{S}$ the time derivative of these, the principle of least action gives the motion of each of the DOF in the system by

$$\frac{d}{dt}\frac{\partial \mathcal{L}}{\partial \dot{s}_n} - \frac{\partial \mathcal{L}}{\partial s_n} = 0 \tag{7.19}$$

For our system the Lagrangian can be defined as $\mathcal{L}(t, S, \dot{S}) = U(t, S) + T(t, \dot{S})$, with

$$T(t, \dot{S}) = \sum_n^{N/2} \frac{1}{2}\left(\frac{1}{m_A} + \frac{1}{m_B}\right)\dot{s}_n^2 \tag{7.20}$$

and

$$U(t, S) = \sum_n^{N/2} \frac{1}{2} k_n \left(\frac{1}{m_A} + \frac{1}{m_B}\right)^2 (s_n(t) - s_{n,0})^2 + \sum_{n,m>n}^{N/2} \sum_{i,j}^{A,B} u_{LJ}^{ij}(r_{i_n,j_m}^2) \tag{7.21}$$

where r_{i_n,j_m}^2 is the squared distance between particles i in molecule n and particle j in molecule m which depends on s_n and s_m and $u_{LJ}^{ij}(r_{i_n,j_m}^2)$ is the Lennard-Jones potential between these particles. From these definitions one can derive an expression for acceleration $d^2 s_n/dt^2$ as a function of S making it possible to get an expression for the dynamics. This will however require a large effort to implement in RUMD, and would probably be better solved by a dedicated software. Besides this, the two methods outlines above only provides an NVE-like ensemble and adding a temperature control would further complicate the methods.

We have chosen to use Monte Carlo simulations. This allows for a relatively simple procedure and automatically assures that the temperature is correct through the Metropolis algorithm, see section 2.2. In order to sample the right micro configurations, we altered the generation of trial moves. Given a configuration $\mathbf{R}$ we created a trial state by changing all the intramolecular distances by a small random number, while keeping orientation and center of mass position of each molecule fixed. The random numbers where taken from a uniform distribution with a mean of 0 and a width of approximately 1/1000 of the natural model spring length. This was done by changing the mass reduced lengths s_n by a displacement δs_n, and then adding it to the Cartesian coordinates of the particles A and B in molecule n as

$$\mathbf{r}_{A_n}^* = \mathbf{r}_{A_n}(t) + \frac{1}{m_A}\delta s_n \hat{\mathbf{r}}_n, \quad \mathbf{r}_{B_n}^* = \mathbf{r}_{B_n}(t) - \frac{1}{m_B}\delta s_n \hat{\mathbf{r}}_n \tag{7.22}$$

This ensures, that the center of mass is fixed, by changing the positions of particles in a molecule relative to their mass and keeps the orientation fixed by adding a vector that is proportional to the normalized orientation of the molecule $\hat{\mathbf{r}}_n$. These trial states are then tested in accordance with the Metropolis algorithm ensuring that the configuration space is sampled in properly. This allows us to perform simulations in the reduced space, where only vibrations occur and calculate the average needed in equation (7.12).

This resulted in the following procedure:

- Run an ordinary NVT-simulation at the reference state point, $(\rho, T) = (1.863, 0.465)$.
- Pick from the simulation a number of configurations, $\mathbf{R}_i$.

- For each of these, do a Monte Carlo simulation, where the trial moves are restricted to those that conserve all molecular centers off mass and orientations.
- Calculate the potential energy U_1 and the scaled potential energy U_2 at given intervals.

7.5 Results of simulations in reduced space

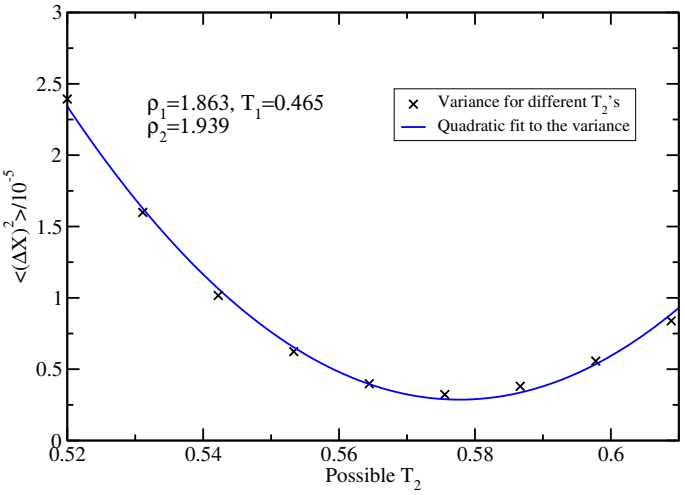

Figure 7.1: The variance of $X(T_2) = F_2^I/k_BT_2 - F_1^I/k_BT_1$ and the quadratic fit to this. Using a quadratic fits makes it possible to estimate the location of the minimum of the variance. The T_2 that corresponds to the minimum in the variance is used as the candidate for the pseudoisomorphic state point.

Applying the method described above, we get the variance of the difference in free energy $\langle(\Delta X)^2\rangle$. This variance is plotted as a function of T_2 on figure 7.1, for the densities $\rho_1 = 1.863$ and $\rho_2 = 1.939$. The minimum in the variance is found at $T_2 = 0.578$. The state point $(\rho_2, T_2) = (1.939, 0.578)$ should then be pseudoisomorphic to the reference state point $(\rho_1, T_1) = (1.863, 0.465)$. This estimate is taken from one simulation, meaning one starting configuration or set of isomorphic DOF. To test the dependence on the chosen configuration in this method we repeated the procedure for a large number of configurations. On figure 7.2 the average predicted T_2 is plotted as a function of the number of simulations run. While the result clearly depends on configuration as seen from the variations when a small number of these are used, the fluctuations are never large with the temperature varying less than a percent. On the figure it seems that after 7500 simulations even these fluctuations disappear leaving statistical noise. It seems the method is rather resilient and we have applied it to a number of density changes.

The temperatures found with this method are shown in table 7.1, where they are compared to the temperatures found to give pseudoisomorphic behaviour in the last chapter. The difference between the predicted temperatures is small showing that the method presented here is a valid one, but they are not exactly the same.

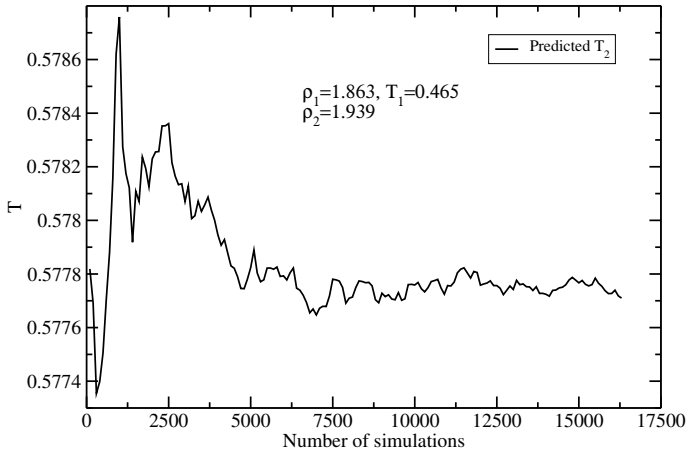

Figure 7.2: The predicted T_2 changes with the number of simulations performed, but the fluctuations are rather small. After 7500 simulations, the temperature is almost fixed.

Table 7.1: The predicted T_2 from the method described in the last chapter with scaled springs T_{SS} and the method used here, equating free energies $T_{2,FE}$

ρ	$T_{2,SS}$	$T_{2,FE}$
1.772	0.352	0.352
1.853	0.465	0.465
1.939	0.577	0.578
2.018	0.711	0.707
2.121	0.915	0.906

To test whether the differences are small enough that they effectively give the same dynamics, we have performed simulations at these state points and calculated the intermediate scattering function for the heavy and light particles, as was done in the previous chapter. Figure 7.3 shows these results and it is clear that there is a collapse, but it is not as good as the one found in the previous chapter. In particular the light particles seems to be affected by the small changes in temperature. Even so, the quality of the collapse shows that the method generates state points with invariant dynamics to a good approximation.

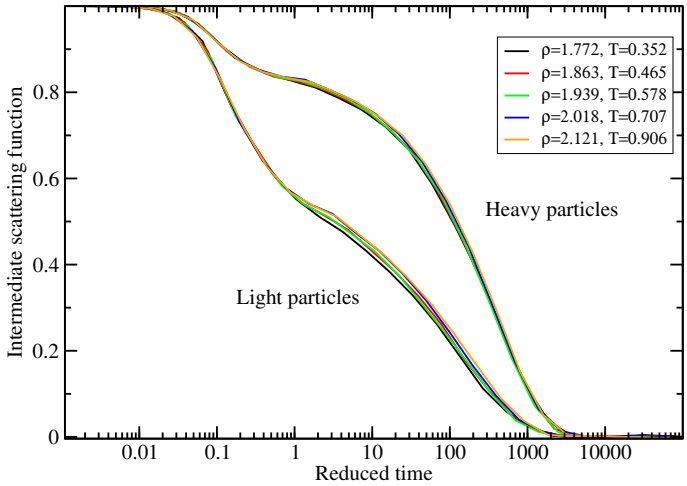

Figure 7.3: The intermediates scattering function for the heavy and light particles along the pseudoisomorph generated by this method calculated with constant reduced q-values. While not perfect, the collapse is rather good

7.6 Harmonic approximation

An alternative way of accessing the free energy of the system relies on the harmonic nature of the intramolecular bonds. Thinking of the systems as done above one can imagine, that the non-isomorphic or vibrational configurational space can be approximated by a set of non-interacting one-dimensional harmonic bonds. If this is the case, the reduced isomorphic free energy F^I/k_BT can be found from the properties of these bonds as shown below.

First we write up the configurational free energy of a system of non-interacting one-dimensional harmonic oscillators

$$\exp[-F_H/k_BT] = \int d\mathbf{X} \exp[-U(\mathbf{X})/k_BT] \tag{7.23}$$

Since we are dealing with harmonic oscillators, we have

$$U(\mathbf{X}) = \sum_i u_{i,0} + \frac{1}{2}k_i(x_i - x_{i,0})^2 \tag{7.24}$$

Because the potential is a sum of independent terms, we can rewrite the expression

for the energy as

$$\begin{aligned}
&\exp[-F_H/k_BT] \\
&= \int dx_1 \dots dx_N \exp\left[-\sum_i \left(u_{i,0} + \frac{1}{2}k_i(x_i - x_{i,0})^2\right)/k_BT\right] \\
&= \int dx_1 \dots dx_N \exp\left[-\sum_i u_{i,0}/k_BT\right] \prod_i \exp\left[-\frac{1}{2}k_i(x_i - x_{i,0})^2/k_BT\right] \\
&= \exp[-U_0/k_BT] \prod_i \int_{-\infty}^{\infty} dx_i \exp\left[-\frac{1}{2}k_i(x_i - x_{i,0})^2\right] \\
&= \exp[-U_0/k_BT] \left(\prod_i \sqrt{\frac{2\pi k_BT}{k_i}}\right)
\end{aligned} \tag{7.25}$$

where $U_0 = \sum_i u_{i,0}$. This gives

$$F_H/k_BT = -U_0/k_BT + N/2\ln(2\pi k_BT) - \frac{1}{2}\sum_i \ln(k_i) \tag{7.26}$$

In our formulation of probabilities in isomorphic space, F_H/k_BT is exactly the needed $F^I(R_I)/k_BT$.

In accordance with equation (7.12) two state points are pseudoisomorphic if

$$-F_1^I(\tilde{R}_I)/k_BT_1 + C = -F_2^I(\tilde{R}_I)/k_BT_2 \tag{7.27}$$

which means that if the harmonic approximation is valid, two state points are pseudoisomorphic if

$$-U_{0,1}/k_BT_1 - \frac{1}{2}\sum_i \ln(k_i^1) + C = -U_{0,2}/k_BT_2 - \frac{1}{2}\sum_i \ln(k_i^2) \tag{7.28}$$

where the term $N/2\ln(2\pi k_BT)$ is included in the general constant C since it is independent of configuration.

Thus in order to find the free energies of the system, we need to know U_0 and k_i.

Since we established in the previous chapter, that the eigenvalues of the potential energy Hessian calculated at an inherent state (IS) separates into a part that related to the springs and a part that does not, one immediate way of accessing k_i could be to take the values of the eigenvalue spectrum that corresponds to the model springs. As a reminder, figure 7.4 shows the eigenvalue spectrum of a single IS for the LJC model and the separation between the high and low strength parts is marked with a green arrow. Recall that the number of eigenvalues in the high strength part of the spectrum matches the number of bonds in the system. As each eigenvalue corresponds to an eigenvector, the assumption of non-interacting one-dimensional oscillators seems reasonable, even though all springs in the LJC model are in fact interacting with at least one other spring.

Using as U_0 the total potential energy of the system at the IS and as the spring strength, the effective springs strengths from the eigenvalues, we get the temperature T_2 from the equation (7.28) as

$$U_{0,2}/k_BT_2 = U_{0,1}/k_BT_1 + (\ln\sum_i k_i^1 - \ln\sum_i k_i^2)/2))^2 + C \tag{7.29}$$

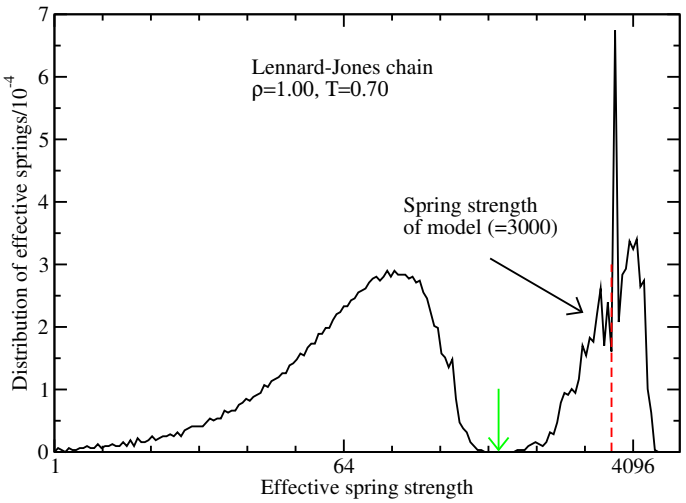

Figure 7.4: The spectrum of the potential energy Hessian eigenvalues for the LJC model. In the previous chapter, we focused on the low strength part of such spectra. Here we focus instead on the high strength parts, presumably corresponding to the model springs. As in figure 6.2 the separation between the two parts are marked with green arrow and the value of the spring strength defined in the model is shown with a dashed red line.

Equation (7.28) only relates two IS, but in this reformulation T_2 can be found from the proportionality between the variance of $U_{0,2}$ and the right hand side of the equation above

$$T_2 = \sqrt{\frac{\langle(\Delta U_{0,2})^2\rangle}{\langle(\Delta(U_{0,1}/k_B T_1 + (\ln\sum_i k_i^1 - \ln\sum_i k_i^2)/2))^2\rangle}} \tag{7.30}$$

Temperatures found in this manner are presented in figure 7.5. The temperatures are shown together with the temperature found in chapter 6, where the invariance of the new L-values was used. Also shown is the temperatures of the configurational adiabat and the empirical formula derived in [66]. The temperatures found with this method matches the temperatures found by the method introduced in the previous chapter and as such is very close to the temperatures of the empirical density scaling as well. Since the temperatures found here are almost identical to those found in the previous chapter, we will not test the invariance of the dynamics.

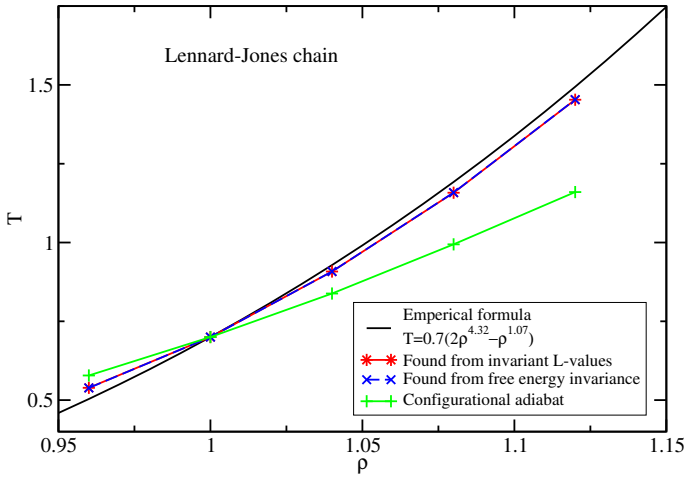

Figure 7.5: The temperatures found from integrating out the vibrational degrees of freedom, using the Hessian of the system, calculated at a number of IS, for the LJC model. Also shown are the temperatures found with the method presented in chapter 6 using the invariance of the L-value. Further more, the temperatures of the configurational adiabat and the empirical formula derived in [66] are shown. The approach of integrating out free energies agree almost completely with the previous result.

7.7 Discussion and conclusion

We have shown that it is possible to estimate pseudoisomorphs from invariance of the reduced isomorphic free energy expressed as

$$-F_2^I(\tilde{R}_I)/k_BT_2 = -F_2^I(\tilde{R}_I)/k_BT_2 + C \tag{7.31}$$

where the isomorphic free energy is given as

$$\exp[-F^I(R_I)/k_BT] = \int dR_{nI} \exp[-U(R_I, R_{nI})/k_BT] \tag{7.32}$$

and R_I and R_{nI} represent the values of the isomorphic and non-isomorphic degrees of freedom.

In particular we showed that through simulations in "vibrational" space it is possible to estimate the pseudoisomorphic state points for the asymmetric dumbbell model. And even though this method does not seem to work as well as the method presented in the previous chapter, it has the added advantage that it does not use the springs directly, so it could be applied to different types of systems, where there are pseudoisomorphs. Further more, it is possible that the specific implementation using Monte Carlo simulations can be modified or replaced with another simulation procedure further increasing the areas of application. It does however have the clear drawback, that it only works because we can physically separate the isomorphic and non-isomorphic degrees of freedom, something that is not necessarily true for other cases.

We have also showed that using a harmonic approximation to the free energy and the eigenvalues of the potential energy Hessian, we can predict pseudoisomorphic state points of the Lennard-Jones chain model with very high precision.

This criteria of invariant free energy opens up a different way of solving the problem of finding pseudoisomorphs.

Ways of accessing the isomorphic free energy can be tailor made to specific systems, meaning that this method might be more robust to application for different kinds of systems with pseudoisomorphs.

There are however some things to consider.

While the results from the Monte Carlo simulations in reduced space are good for the asymmetric dumbbell model, it is not clear how such a method should be generalized even to the Lennard-Jones chain model. Is it the orientation that should be fixed? Defined naively as the end-to-end vector, it seems to be a rather arbitrary quantity to fix. Is the end-to-end vector more defining of the system than the vector from the first to the second-to-last particle in the chain? The problem only gets more complicated if one imagines a cyclic molecule.

As for the pseudoisomorphs of the LJC, they relied, as in last chapter on the separation of the eigenvalue spectrum, though in a completely different way than before. This means, as alluded to earlier, that we do not have a final procedure for finding pseudoisomorphic state points in a general system with pseudoisomorphs.

Even so, given that the problem of identifying isomorphs in systems with harmonic bonds have been known for nearly as long as the isomorph theory it self, the results presented in this thesis must be considered a step in the right direction.

Bibliography

[1] Dan E. Albrechtsen, Andreas E. Olsen, Ulf R. Pedersen, Thomas B. Schrøder, and Jeppe C. Dyre. Isomorph invariance of the structure and dynamics of classical crystals. *Phys. Rev. B*, 90:094106, Sep 2014.

[2] M. P. Allen and D. J. Tildesley. *Computer simulations of liquids*. Oxford University Press, 1987.

[3] N.W. Ashcroft and N.D. Mermin. *Solid State Physics*. Cengage Learning, 2011.

[4] Andreas K. Bacher, Thomas B. Schrøder, and Jeppe C. Dyre. Explaining why simple liquids are quasi-universal. *Nature Communications*, 5:5424, 11 2014.

[5] N. P. Bailey, U. R. Pedersen, N. Gnan, T. B. Schrøder, and J. C. Dyre. Pressure-energy correlations in liquids. I. Results from computer simulations. *J. Chem. Phys.*, 129:184507, 2008.

[6] N. P. Bailey, U. R. Pedersen, N. Gnan, T. B. Schrøder, and J. C. Dyre. Pressure-energy correlations in liquids. II. Analysis and consequences. *J. Chem. Phys.*, 129:184508, 2008.

[7] Nicholas P. Bailey, Trond S. Ingebrigtsen, Jesper Schmidt Hansen, Arno A. Veldhorst, Lasse Bøhling, Claire A. Lemarchand, Andreas E. Olsen, Andreas K. Bacher, Heine Larsen, Jeppe C. Dyre, and Thomas B. Schrøder. Rumd: A general purpose molecular dynamics package optimized to utilize gpu hardware down to a few thousand particles, 2015.

[8] Charles H Bennett. Efficient estimation of free energy differences from monte carlo data. *Journal of Computational Physics*, 22(2):245–268, 1976.

[9] H. J. C. Berendsen, J. R. Grigera, and T. P. Straatsma. The missing term in effective pair potentials. *The Journal of Physical Chemistry*, 91(24):6269–6271, 1987.

[10] P. G. Bolhuis and C. Dellago. Practical and conceptual path sampling issues. *The European Physical Journal Special Topics*, 224(12):2409–2427, 2015.

[11] R. A. Buckingham. The classical equation of state of gaseous helium, neon and argon. *Proceedings of the Royal Society of London A: Mathematical, Physical and Engineering Sciences*, 168(933):264–283, 1938.

[12] R. Casalini and C. M. Roland. Thermodynamical scaling of the glass transition dynamics. *Phys. Rev. E*, 69:062501, Jun 2004.

[13] YuHong Dai and YaXiang Yuan. Alternate minimization gradient method. *IMA Journal of Numerical Analysis*, 23(3):377–393, 2003.

[14] Pablo G. Debenedetti and Frank H. Stillinger. Supercooled liquids and the glass transitio. *Nature*, 410:259–267, Mar 2001.

[15] J. C. Dyre. Colloquium: The glass transition and elastic models of glass-forming liquids. *Rev. Mod. Phys.*, 78:953–972, 2006.

[16] J. C. Dyre and Andreas Kvist Bacher. The mother of all pair potentials. *Colloid and Polymer Science*, 292(8):1971–1975, 2014.

[17] Jeppe C. Dyre. Hidden scale invariance in condensed matter. *The Journal of Physical Chemistry B*, 118(34):10007–10024, 2014. PMID: 25011702.

[18] M. Dzugutov. A universal scaling law for atomic diffusion in condensed matter. *Nature*, 381:137–139, 1996.

[19] Roger Edberg, Denis J. Evans, and G. P. Morriss. Constrained molecular dynamics: Simulations of liquid alkanes with a new algorithm. *The Journal of Chemical Physics*, 84(12):6933–6939, 1986.

[20] M. D. Ediger and Peter Harrowell. Perspective: Supercooled liquids and glasses. *The Journal of Chemical Physics*, 137(8), 2012.

[21] Denis J. Evans, William G. Hoover, Bruce H. Failor, Bill Moran, and Anthony J. C. Ladd. Nonequilibrium molecular dynamics via gauss's principle of least constraint. *Phys. Rev. A*, 28:1016–1021, Aug 1983.

[22] D. Frenkel and B. Smit. *Understanding Molecular Simulation*. Academic Press, 2 edition, 2002.

[23] Nicoletta Gnan, Thomas B. Schrøder, Ulf R. Pedersen, Nicholas P. Bailey, and Jeppe C. Dyre. Pressure-energy correlations in liquids. iv. isomorphs in liquid phase diagrams. *The Journal of Chemical Physics*, 131(23), 2009.

[24] Ditte Gundermann, Ulf R. Pedersen, Tina Hecksher, Nicholas P. Bailey, Bo Jakobsen, Tage Christensen, Niels B. Olsen, Thomas B. Schroder, Daniel Fragiadakis, Riccardo Casalini, C. Michael Roland, Jeppe C. Dyre, and Kristine Niss. Predicting the density-scaling exponent of a glass-forming liquid from prigogine-defay ratio measurements. *Nature Physics*, 7(10):816–821, 2011.

[25] J. S. Hansen, Thomas B. Schrøder, and Jeppe C. Dyre. Simplistic coulomb forces in molecular dynamics: Comparing the wolf and shifted-force approximations. *The Journal of Physical Chemistry B*, 116(19):5738–5743, 2012. PMID: 22497264.

[26] Jean-Pierre Hansen and Ian R. McDonald. *Theory of Simple Liquids (Third Edition)*. Academic Press, Burlington, third edition edition, 2006.

[27] D. M. Heyes, D. Dini, and A. C. Braka. Scaling of lennardjones liquid elastic moduli, viscoelasticity and other properties along fluidsolid coexistence. *physica status solidi (b)*, 252(7):1514–1525, 2015.

[28] T. S. Ingebrigsten, T. B. Schrøder, and J. C. Dyre. Isomorphs in model molecular liquids. *J. Phys. Chem. B*, 116:1018–1034, 2012.

[29] Trond S. Ingebrigtsen, Thomas B. Schrøder, and Jeppe C. Dyre. Isomorphs in model molecular liquids. *The Journal of Physical Chemistry B*, 116(3):1018–1034, 2012. PMID: 22251282.

[30] C. Kittel. *Introduction to Solid State Physics*. Wiley, 2004.

[31] Jennifer L. Knight and Charles L. Brooks. -dynamics free energy simulation methods. *Journal of Computational Chemistry*, 30(11):1692–1700, 2009.

[32] Walter Kob and Hans C. Andersen. Scaling behavior in the β-relaxation regime of a supercooled lennard-jones mixture. *Phys. Rev. Lett.*, 73:1376–1379, Sep 1994.

[33] L. D. Landau and E. M. Lifshitz. *Course of Theoretical Physics – Volume 1*. Butterworth-Heinemann, Oxford, third edition edition, 1976.

[34] J. E. Lennard Jones. On the Determination of Molecular Fields. I. From Variation of the Viscosity of a Gas with Temperature. *Proceedings of the Royal Society of London A: Mathematical, Physical and Engineering Sciences*, 106(738):441–462, 1924.

[35] Laurent J. Lewis and Göran Wahnström. Molecular-dynamics study of supercooled *ortho* -terphenyl. *Phys. Rev. E*, 50:3865–3877, Nov 1994.

[36] E. R. López, A. S. Pensado, M. J. P. Comuñas, A. A. H. Pádua, J. Fernández, and K. R. Harris. Density scaling of the transport properties of molecular and ionic liquids. *J. Chem. Phys.*, 134:144507, 2011.

[37] Nicholas Metropolis, Arianna W. Rosenbluth, Marshall N. Rosenbluth, Augusta H. Teller, and Edward Teller. Equation of state calculations by fast computing machines. *The Journal of Chemical Physics*, 21(6):1087–1092, 1953.

[38] Andreas Elmerdahl Olsen and Dan Elmkvist Albrechtsen. Isomorfer i krystaller, 2013.

[39] Ulf R. Pedersen, Nicholas P. Bailey, Thomas B. Schrøder, and Jeppe C. Dyre. Strong pressure-energy correlations in van der waals liquids. *Phys. Rev. Lett.*, 100:015701, Jan 2008.

[40] Ulf R. Pedersen, Tage Christensen, Thomas B. Schrøder, and Jeppe C. Dyre. Feasibility of a single-parameter description of equilibrium viscous liquid dynamics. *Phys. Rev. E*, 77:011201, Jan 2008.

[41] Ulf R. Pedersen, Thomas B. Schrøder, Jeppe C. Dyre, and Peter Harrowell. Geometry of slow structural fluctuations in a supercooled binary alloy. *Phys. Rev. Lett.*, 104:105701, Mar 2010.

[42] D. C. Rapaport. *The art of Molecular Dynamics simulation*. Cambridge University Press, 2 edition, 2004.

[43] Marcos Raydan. On the barzilai and borwein choice of steplength for the gradient method. *IMA Journal of Numerical Analysis*, 13(3):321–326, 1993.

[44] Lisa Anita Roed, Ditte Gundermann, Jeppe C. Dyre, and Kristine Niss. Communication: Two measures of isochronal superposition. *Journal of Chemical Physics*, 139(10):101101, 2013.

[45] C. M. Roland, R. B. Bogoslovov, R. Casalini, A. R. Ellis, S. Bair, S. J. Rzoska, K. Czuprynski, and S. Urban. Thermodynamic scaling and the characteristic relaxation time at the phase transition of liquid crystals. *J. Chem. Phys.*, 128:224506, 2008.

[46] C M Roland, S Hensel-Bielowka, M Paluch, and R Casalini. Supercooled dynamics of glass-forming liquids and polymers under hydrostatic pressure. *Reports on Progress in Physics*, 68(6):1405, 2005.

[47] Y. Rosenfeld. A quasi-universal scaling law for atomic transport in simple fluids. *J. Phys.: Condens. Matter*, 11:5415–5427, 1999.

[48] Srikanth Sastry. Liquid limits: Glass transition and liquid-gas spinodal boundaries of metastable liquids. *Phys. Rev. Lett.*, 85:590–593, Jul 2000.

[49] Srikanth Sastry. The relationship between fragility, configurational entropy and the potential energy landscape of glass-forming liquids. *Nature*, 409:164–167, 2001.

[50] T. B. Schrøder, N. P. Bailey, U. R. Pedersen, N. Gnan, and J. C. Dyre. Pressure-energy correlations in liquids. III. Statistical mechanics and thermodynamics with hidden scale invariance. *J. Chem. Phys.*, 131(23):234504, 2009.

[51] T. B. Schrøder, N. Gnan, U. R. Pedersen, N. P. Bailey, and J. C. Dyre. Pressure-energy correlations in liquids. V. Isomorphs in generalized Lennard-Jones systems. *J. Chem. Phys.*, 134(16):164505, 2011.

[52] Thomas Schrøder and J. C. Dyre. Simplicity of condensed matter at its core: Generic definition of a roskilde-simple system. *Journal of Chemical Physics*, 141, 2014.

[53] Thomas B. Schrøder, Ulf R. Pedersen, Nicholas P. Bailey, Søren Toxvaerd, and Jeppe C. Dyre. Hidden scale invariance in molecular van der waals liquids: A simulation study. *Phys. Rev. E*, 80:041502, Oct 2009.

[54] F. Sciortino, W. Kob, and P. Tartaglia. Inherent structure entropy of supercooled liquids. *Phys. Rev. Lett.*, 83:3214–3217, Oct 1999.

[55] David E. Smith and Liem X. Dang. Computer simulations of nacl association in polarizable water. *The Journal of Chemical Physics*, 100(5):3757–3766, 1994.

[56] A. Tölle, H. Schober, J. Wuttke, O. G. Randl, and F. Fujara. Fast relaxation in a fragile liquid under pressure. *Phys. Rev. Lett.*, 80:2374–2377, Mar 1998.

[57] Albert Tölle. Neutron scattering studies of the model glass former ortho - terphenyl. *Reports on Progress in Physics*, 64(11):1473, 2001.

[58] Søren Toxvaerd and Jeppe C. Dyre. Communication: Shifted forces in molecular dynamics. *The Journal of Chemical Physics*, 134(8), 2011.

[59] Søren Toxvaerd, Ole J. Heilmann, and Jeppe C. Dyre. Energy conservation in molecular dynamics simulations of classical systems. *The Journal of Chemical Physics*, 136(22), 2012.

[60] Søren Toxvaerd, Ole J. Heilmann, Trond Ingebrigtsen, Thomas B. Schrøder, and Jeppe C. Dyre. Time-reversible molecular dynamics algorithms with bond constraints. *The Journal of Chemical Physics*, 131(6), 2009.

[61] Benjamin W van de Waal. Can the lennard-jones solid be expected to be fcc? *Physical review letters*, 67(23):3263, 1991.

[62] S. van der Walt, S. C. Colbert, and G. Varoquaux. The numpy array: A structure for efficient numerical computation. *Computing in Science Engineering*, 13(2):22–30, March 2011.

[63] A. A. Veldhorst, L. Bøhling, J. C. Dyre, and T. B. Schrøder. Isomorphs in the phase diagram of a model liquid without inverse power law repulsion. *The European Physical Journal B*, 85(1):1–7, 2012.

[64] Arno Veldhorst. *Tests of the isomorph theory by computer simulations of atomic and molecular model liquids*. PhD thesis, Roskilde University, 2014.

[65] Arno A. Veldhorst, Jeppe C. Dyre, and Thomas B. Schrøder. Scaling of the dynamics of flexible lennard-jones chains. *The Journal of Chemical Physics*, 141(5), 2014.

[66] Arno A. Veldhorst, Jeppe C. Dyre, and Thomas B. Schrøder. Scaling of the dynamics of flexible lennard-jones chains: Effects of harmonic bonds. *The Journal of Chemical Physics*, 143(19), 2015.

[67] Arno A. Veldhorst, Thomas B. Schrøder, and Jeppe C. Dyre. Invariants in the Yukawa system's thermodynamic phase diagram. *Physics of Plasmas*, 22:073705, 2015.

[68] Loup Verlet. Computer "experiments" on classical fluids. i. thermodynamical properties of lennard-jones molecules. *Phys. Rev.*, 159:98–103, Jul 1967.

[69] Göran Wahnström. Molecular-dynamics study of a supercooled two-component lennard-jones system. *Phys. Rev. A*, 44:3752–3764, Sep 1991.

[70] David J. Wales. *Energy Landscapes - with application to clusters, biomolecules and glasses*. Cambridge Molecular science, Cambridge, first edition edition, 2003.

[71] Wence Xiao, Jon Tofteskov, Troels V. Christensen, Jeppe C. Dyre, and Kristine Niss. Isomorph theory prediction for the dielectric loss variation along an isochrone. *Journal of Non-Crystalline Solids*, 407(0):190 – 195, 2015. 7th IDMRCS: Relaxation in Complex Systems.